JOURNAL OF GEOPHYSICAL RESEARCH, VOL. 112, F03S28, doi:10.1029/2006JF000664, 2007

Ice sheet grounding line dynamics: Steady states, stability, and hysteresis

Christian Schoof[1]

Received 21 August 2006; revised 17 November 2006; accepted 1 March 2007; published 14 July 2007.

[1] The ice sheet–ice shelf transition zone plays an important role in controlling marine ice sheet dynamics, as it determines the rate at which ice flows out of the grounded part of the ice sheet. Together with accumulation, this outflow is the main control on the mass balance of the grounded sheet. In this paper, we verify the results of a boundary layer theory for ice flux in the transition zone against numerical solutions that are able to resolve the transition zone. Very close agreement is obtained, and grid refinement in the transition zone is identified as a critical component in obtaining reliable numerical results. The boundary layer theory confirms that ice flux through the grounding line in a two-dimensional sheet-shelf system increases sharply with ice thickness at the grounding line. This result is then applied to the large-scale dynamics of a marine ice sheet. Our principal results are that (1) marine ice sheets do not exhibit neutral equilibrium but have well-defined, discrete equilibrium profiles; (2) steady grounding lines cannot be stable on reverse bed slopes; and (3) marine ice sheets with overdeepened beds can undergo hysteresis under variations in sea level, accumulation rate, basal slipperiness, and ice viscosity. This hysteretic behavior can in principle explain the retreat of the West Antarctic ice sheet following the Last Glacial Maximum and may play a role in the dynamics of Heinrich events.

Citation: Schoof, C. (2007), Ice sheet grounding line dynamics: Steady states, stability, and hysteresis, *J. Geophys. Res.*, *112*, F03S28, doi:10.1029/2006JF000664.

1. Introduction

[2] Ice sheets grounded on bedrock below sea level can play a pivotal role in the Earth's climate system. They are not merely large bodies of frozen fresh water whose release would impact albedo, ocean circulation and sea levels, but they also respond sensitively to changes in the surrounding oceans. Warming in the Amundsen sea [*Payne et al.*, 2004] and the collapse of ice shelves in the Antarctic Peninsula [*Rignot et al.*, 2004] have led to marked changes in the flow of grounded ice in West Antarctica, where much of the ice sheet bed is below sea level, while the collapse of a much larger ice sheet on the West Antarctic continental shelf following the Last Glacial Maximum may have been triggered by sea level rise due to the melting of ice sheets in the Northern Hemisphere [*Conway et al.*, 1999]. Marine triggers have also been suggested for massive discharges of ice from the Laurentide ice sheet during the last ice age, also known as Heinrich events [*Clarke et al.*, 1999; *Flückiger et al.*, 2006].

[3] The purpose of this paper is to develop an improved theory for marine ice sheet dynamics based on the physics of the ice sheet–ice shelf transition zone. Our work builds on a substantial literature which has identified coupling between ice sheet and ice shelves as an essential control on the dynamics of marine ice sheets [e.g., *Weertman*, 1974; *Thomas and Bentley*, 1978; *van der Veen*, 1985; *MacAyeal*, 1987; *Herterich*, 1987; *Hindmarsh*, 1993, 1996, 2006; *Chugunov and Wilchinsky*, 1996; *Dupont and Alley*, 2005; *Vieli and Payne*, 2005; *Pattyn et al.*, 2006; *Schoof*, 2007].

[4] Mechanically, grounded ice sheet flow is dominated by vertical shear, while ice shelf flow is a buoyancy-driven flow dominated by longitudinal stretching and lateral shearing. The two types of flow couple together across a complex mechanical transition zone near the grounding line in which longitudinal and shear stresses are important. The dynamic role of this transition zone is that it controls the rate of outflow of ice across the grounding line. Along with net accumulation, outflow of ice is the main control on the mass balance of the grounded part of a marine ice sheet. By contrast, mass loss from floating ice shelves through calving and basal melting does not affect the grounded sheet directly. Instead, these processes alter the geometry of the ice shelf, which affects the grounded sheet only through mechanical coupling across the grounding line (Figure 1).

[5] In order to understand the dynamics of the grounded part of a marine ice sheet (which controls its contribution to sea level change), it is therefore essential to understand the behavior of the sheet-shelf transition zone. The horizontal extent of the transition zone is the distance over which longitudinal stresses from the ice shelf propagate into the ice sheet. This distance is frequently on the subgrid scale in numerical ice sheet models and in some cases it may only

[1]Department of Earth and Ocean Sciences, University of British Columbia, Vancouver, British Columbia, Canada.

0148-0227/07/2006JF000664$09.00

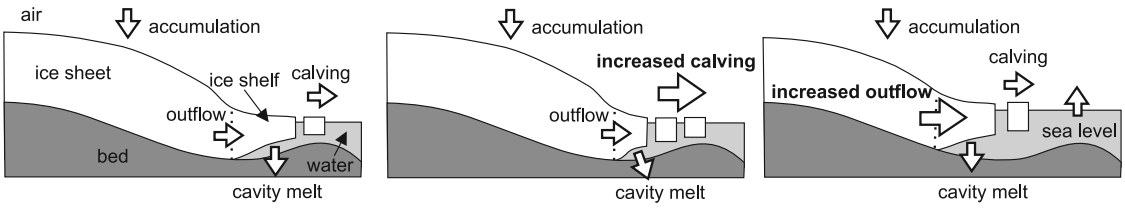

Figure 1. Main components in the mass balance of a marine ice sheet. Increased calving and shelf cavity melting affect only the mass of floating ice and are sea level neutral. Increased outflow through the grounding ice and accumulation control grounded ice volume and hence the effect of the ice sheet on sea levels.

be a few ice thicknesses in length [e.g., *Chugunov and Wilchinsky*, 1996]. However, this in no way implies that the transition zone can be ignored in an ice sheet model.

[6] On the basis of a boundary layer theory by *Schoof* [2007], we show in this paper how the effect of the narrow transition zone can be parameterized in a large-scale ice sheet model that does not resolve the transition zone, and demonstrate that this parameterization agrees with the results of a numerical model that resolves the transition zone through grid refinement. We then apply this theory to the large-scale dynamics of marine ice sheets.

[7] Our main concern will be with marine ice sheet instability. Briefly, the marine ice sheet instability hypothesis [*Weertman*, 1974; *Thomas and Bentley*, 1978] asserts that ice discharge through the grounding line should increase with ice thickness there. Suppose then that a steady marine ice sheet has its grounding line located on an upward sloping bed. A slight retreat in grounding line position will lead to an increase in ice thickness and hence ice discharge at the grounding line. This represents a positive feedback: the increase in ice discharge should lead to a further shrinkage in the ice sheet and hence grounding line retreat, leading to a further increase in ice discharge and so on (a similar feedback underlies the rapid retreat of tidewater glaciers) [see *Meier and Post*, 1987]. This feedback should continue until the ice sheet either disintegrates completely or stabilizes in a region with a downward sloping bed, where the reverse of the instability mechanism applies: steady profiles on downward slopes should be stable to small perturbations.

[8] According to the instability hypothesis, stable grounding lines therefore cannot be located on upward sloping portions of seafloor. This is especially relevant to West Antarctica. The ice sheet bed near the center of West Antarctica is deeper than at the grounding line, suggesting the current ice sheet may not be stable. More precisely, it suggests that the ice sheet is unlikely to be in a steady state.

[9] There is also evidence of a much larger ice sheet that covered the seafloor in the Ross and Ronne-Filchner embayments during the Last Glacial Maximum, and may have extended to the shallow Antarctic continental shelf edge [*Conway et al.*, 1999; *Wellner et al.*, 2001; *Stone et al.*, 2003], and its retreat may have been linked to marine ice sheet instability. In addition, the instability mechanism raises the possibility of triggering irreversible grounding line retreat where there are overdeepenings close to grounding lines. This has been considered as a possible explanation for Heinrich events [e.g., *Clarke et al.*, 1999; *Hulbe et al.*, 2004], and has implications for the current configuration of Antarctica. Present-day overdeepenings there which may be susceptible to grounding line retreat include the widely studied Pine Island Glacier [e.g., *Rignot et al.*, 2002; *Schmeltz et al.*, 2002; *Payne et al.*, 2004].

[10] The original theory for marine ice sheet instability [*Weertman*, 1974; *Thomas and Bentley*, 1978] has, however, been controversial. The papers by Weertman and by Thomas and Bentley offer a somewhat simplistic description of the transition between grounded sheet and floating shelf, and it is unclear whether they provide the correct prescription for the rate of mass loss from the grounded sheet. Indeed, *Hindmarsh* [1993, 1996] has argued that the coupling between sheet and shelf should have a negligible impact on the dynamics of the grounded ice sheet, and goes on to hypothesize that steady marine ice sheets should be neutrally stable to changes in grounding line position. In effect, Hindmarsh argues that the transition zone does not uniquely determine the mass flux out of the grounded sheet, in contradiction to what we have stated above, and that a steady marine ice sheet should be neutrally stable to displacements in grounding line position. The implication of this argument is that there should be an infinite number of steady marine ice sheet profiles.

[11] More recently, *Hindmarsh* [2006] has modified this argument somewhat, demonstrating that certain combinations of steady state ice thickness and ice flux at the grounding line are not physically possible. As a result, he proposes that some grounding line positions cannot correspond to steady marine ice sheets, but that all grounding line positions within a certain ''permissible'' spatial range can be steady and neutrally stable to perturbations. Numerical work by *Vieli and Payne* [2005] and *Pattyn et al.* [2006] has not been able to resolve the stability issue unequivocally. Although these authors were unable to find steady state solutions on upward sloping beds, they did raise the possibility of neutral equilibrium on downward sloping beds.

[12] The present paper is motivated by a boundary layer theory for the sheet-shelf transition zone described by *Schoof* [2007]. This theory demonstrates that it is mathematically possible to calculate ice flux across the grounding line by integrating a local ice flow problem close to the grounding line. This result stands in contrast with the assertions of *Hindmarsh* [1993, 1996, 2006] to the contrary, and qualitatively confirms the conjectures of *Weertman* [1974] and *Thomas and Bentley* [1978]. In particular, the boundary layer theory predicts that a marine ice sheet can only have a finite number of steady surface profiles, and that these cannot be neutrally stable.

[13] The scope of the present paper is threefold. The first two objectives are technical and aimed at model improve-

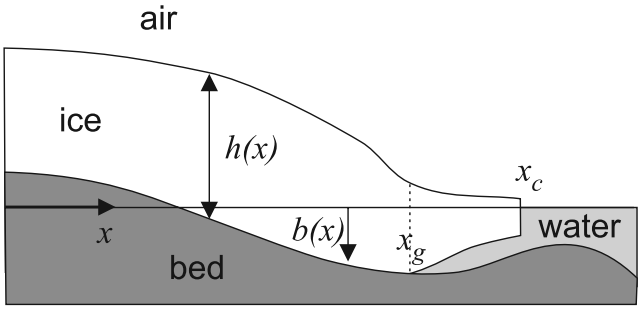

Figure 2. Geometry of the problem.

ment, while the third takes a broader view of marine ice sheet dynamics. First, we will use numerical solutions of a marine ice sheet model to verify the boundary layer results constructed by *Schoof* [2007]. Simultaneously, we exploit the boundary layer theory to provide a reproducible benchmark for numerical solutions. This is a timely exercise in view of the inconsistent results produced by recent, numerical marine ice sheet studies, which indicate that numerical artifacts may be a significant issue [*Vieli and Payne*, 2005].

[14] The third and main purpose of the paper is to study marine ice sheet stability. We use our numerical results in conjunction with boundary layer theory to study how physical and climatic parameters such sea level, accumulation rates, sliding rates and ice viscosity affect steady ice sheet profiles, and to discuss the stability of these profiles to small perturbations. It is worth underlining that the concept of "stability" is only useful here when applied to steady profiles, in which case it also has a well-defined mathematical meaning. In practical terms, any unsteady profile is unlikely to be considered "stable."

[15] Ice sheets are, in general, not necessarily in a steady state. However, the general dynamics of ice sheets are diffusive in the mathematical sense: in the simplest realistic ("shallow ice") models, ice thickness evolves according to a diffusion equation. Diffusive systems tend to relax to a steady state. By studying steady states and their stability properties, a great deal can therefore be learnt about ice sheet dynamics, notably about long-timescale behavior: is a particular steady profile viable in the long term or not? Is there a single profile the ice sheet will relax to, or are there several, and what initial conditions are required to attain each of these steady profiles? Does an ice sheet undergo hysteresis under slowly varying external forcing?

[16] In the next section, we describe the simplest possible model which is able to describe the behavior of the transition zone as well as the interior of the ice sheet and the flow of the attached ice shelf by taking account of both dominant stress components.

2. Model

2.1. Coupled Sheet-Shelf Flow

[17] Our model is a depth-integrated model for the flow of a rapidly sliding, two-dimensional symmetrical marine ice sheet [e.g., *Muszynski and Birchfield*, 1987; *MacAyeal*, 1989]. It is the simplest model which allows both vertical and longitudinal stress in the ice to be resolved, but has the drawback of not including the contribution of shearing to ice flux in the grounded sheet.

[18] Let h be ice thickness and u ice velocity, while b is the depth of the ice sheet bed below sea level and x is horizontal position (see Figure 2). Then mass and momentum conservation require, respectively,

$$\frac{\partial h}{\partial t}+\frac{\partial (hu)}{\partial x}=a \tag{1}$$

$$\frac{\partial}{\partial x}\left[2\bar{A}^{-1/n}h\left|\frac{\partial u}{\partial x}\right|^{1/n-1}\frac{\partial u}{\partial x}\right]-C|u|^{m-1}u-\rho_i g h\frac{\partial (h-b)}{\partial x}=0. \tag{2}$$

Here, ρ_i and g are ice density and acceleration due to gravity, respectively, while $\bar{A}$ is the depth-averaged temperature-dependent rheological coefficient A in Glen's law [*Paterson*, 1994, chapter 5], and n is the corresponding exponent. (If z is depth in the ice sheet, then $\bar{A}^{-1/n}=h^{-1}\int_{-b}^{h-b}[A(z)]^{-1/n}\,\mathrm{d}z$.)

[19] In equation (1), a is ice accumulation rate. The first term in the momentum balance equation (2) represents the effect of longitudinal stresses in the ice. Even though we expect these stresses to be insignificant in the interior of the ice sheet, we retain them here because they must play an important role in the flow of ice in the transition zone near the grounding line. The second term in equation (2) represents the effect of vertical shear stresses. More precisely, the second term represents friction at the bed (assumed to depend on sliding velocity u as $\tau_b=C|u|^{m-1}u$) [see *Weertman*, 1957; *Fowler*, 1981], which balances vertical shear stress. (Note that although vertical shear stress therefore features at leading order in force balance, the contribution of vertical shearing to ice velocity is assumed to be small compared with sliding velocities.) The last term in equation (2) is simply the driving stress: the term $\partial(h-b)/\partial x$ is the surface slope of the ice sheet. Note that we have defined b to be positive if the bed is below sea level; that is, depth of the bed is measured downward.

[20] The center of the symmetrical ice sheet is located at $x=0$. Symmetry implies that

$$\frac{\partial (h-b)}{\partial x}=u=0 \qquad \text{at} \qquad x=0. \tag{3}$$

[21] At the grounding line position, $x=x_g$, we couple the ice sheet model to an ice shelf model. The ice shelf satisfies mass and momentum balance relations analogous to equations (1) and (2) [e.g., *MacAyeal and Barcilon*, 1988]:

$$\frac{\partial h}{\partial t}+\frac{\partial (hu)}{\partial x}=a \tag{4}$$

$$\frac{\partial}{\partial x}\left[2\bar{A}^{-1/n}h\left|\frac{\partial u}{\partial x}\right|^{1/n-1}\frac{\partial u}{\partial x}\right]-\rho_i(1-\rho_i/\rho_w)gh\frac{\partial h}{\partial x}=0, \tag{5}$$

where ρ_w is the density of water. Two points are worth noting. First, there is no basal friction in ice shelves, so the $C|u|^{m-1}u$ term is missing. Second, the driving stress $(1-\rho_i/\rho_w)\rho_i g h\partial h/\partial x$ would be zero if ice and water had the same density. This underlines that the flow of ice shelves is buoyancy driven.

[22] At the grounding line, we assume that ice flux, ice thickness and longitudinal stress, and hence h, u and $\partial u/\partial x$ are continuous. The ice also begins to float at the grounding line, and so

$$\rho_i h = \rho_w b \qquad \text{at} \qquad x = x_g. \tag{6}$$

[23] At the calving front, there is an imbalance between hydrostatic pressures in ice and water due to the buoyancy of ice. This imbalance must be compensated by a longitudinal stress [e.g., *Shumskiy and Krass*, 1976]:

$$2\bar{A}^{-1/n} h \left|\frac{\partial u}{\partial x}\right|^{1/n-1} \frac{\partial u}{\partial x} = \frac{1}{2}\rho_i g\left(1 - \frac{\rho_i}{\rho_w}\right)h^2 \qquad \text{at } x = x_c. \tag{7}$$

[24] To complete the model for the ice shelf, we also need a calving condition for mass loss at the edge of the ice shelf. Possible forms for calving rates are given by *van der Veen* [1996], though these are poorly constrained. Fortuitously, we can avoid this issue. Our objective is solely to understand the dynamics of grounded ice, and this is unaffected by the details of calving from the shelf in a two-dimensional ice sheet. In fact, we will see in the next subsection that the ice shelf model above is completely passive in the dynamics of the grounded ice, and therefore the calving rate does not affect grounded ice flow. Hence, possibly surprisingly, we do not need to prescribe a calving rate here, provided we only study the behavior of the grounded ice, upstream of the grounding line.

2.2. Integration of Shelf Flow

[25] The calculation below may also be found in work by *MacAyeal and Barcilon* [1988], but is worth repeating to underline the point: A two-dimensional shelf has no effect on the dynamics of the grounded ice upstream of it. We emphasize, however, that this only holds for a two-dimensional ice shelf, provided it is freely floating and has no ice rumples (see also sections 4.2 and 4.3).

[26] This statement assumes that there is no contact between shelf and seafloor (no ice rumples) that could generate basal friction on the shelf, as implied by equation (5). To prove it, we use the fact that $h\partial h/\partial x = 2^{-1}\partial(h^2)/\partial x$ to rewrite equation (5) as

$$\frac{\partial}{\partial x}\left[2\bar{A}^{-1/n} h \left|\frac{\partial u}{\partial x}\right|^{1/n-1} \frac{\partial u}{\partial x} - \frac{1}{2}\rho_i\left(1 - \frac{\rho_i}{\rho_w}\right)gh^2\right] = 0. \tag{8}$$

This shows that the term in square brackets must remain constant in the shelf, and from equation (7), we deduce that it must equal zero everywhere in the shelf. Hence equation (7) must in fact hold everywhere in the shelf. Because h and $\partial u/\partial x$ are continuous at $x = x_g$, this implies that

$$2\bar{A}^{-1/n} h \left|\frac{\partial u}{\partial x}\right|^{1/n-1} \frac{\partial u}{\partial x} = \frac{1}{2}\rho_i\left(1 - \frac{\rho_i}{\rho_w}\right)gh^2 \qquad \text{at} \quad x = x_g. \tag{9}$$

The longitudinal stress at the grounding line is simply a function of ice thickness there, regardless of the shape of the ice shelf.

[27] As a result, we can add the stress condition (9) to the flotation condition (6) as boundary conditions at the grounding line. This is all we need to describe the coupling between sheet and shelf, and the actual dynamics of the shelf are irrelevant to the grounded sheet. No further boundary conditions are required, either to evolve ice thickness or to determine grounding line migration. We use the scheme described in detail in Appendix A to solve the mass and momentum balance equations (1), (2) with boundary conditions (3), (6) and (9). We will call this the "full model" to distinguish it from the boundary layer models described later, and point out that our numerical scheme for solving it is specially adapted to resolve the sheet-shelf transition zone.

3. Results

[28] Our aim is to analyze equations (1), (2), (3), (6) and (9) (the full model) as the simplest possible physics-based marine ice sheet model that can resolve the sheet-shelf transition. We have not attempted to include effects such as lateral shearing or buttressing in our two-dimensional model. Our motivation is to set out clearly how a two-dimensional ice sheet behaves, and to generate a reproducible benchmark against which other models, which may include these additional and undoubtedly significant effects, can be tested. In the same spirit, we assume constant values for the material parameters C and $\bar{A}$.

[29] Constant C is important because we do not prescribe a length scale for the sheet-shelf transition zone through variations in C, as is done by, e.g., *van der Veen* [1985] and *Pattyn et al.* [2006]. In our paper, the size of the transition zone is determined by the model parameters C and $\bar{A}$ and the geometry of the ice sheet bed, see *Schoof* [2007] and equation (A9) in Appendix A below. (By contrast, *van der Veen* [1985] arbitrarily and somewhat unphysically imposes a distance from the grounding line beyond which longitudinal stress $2\bar{A}^{-1/n}h|\partial u/\partial\, x|^{1/n-1}\partial u/\partial x$ must vanish. *Pattyn et al.* [2006] indirectly introduce a length scale by imposing strong spatial variations in the basal friction parameter near the grounding line, of the form $C \propto \exp(\beta_0(x_g - x))$, so that β_0^{-1} is a natural transition zone length scale.)

[30] To give a flavor of our results, we compute the relaxation to steady state of a marine ice sheet described by the "full model" (see end of section 2.1). In keeping with our results from section 2.1 we only display the grounded part of the ice sheet. The synthetic bed shape used has a central portion above sea level, an overdeepening, and a shallow sill close to the continental shelf edge:

$$b(x) = -\left[729 - 2184.8 \times \left(\frac{x}{750\text{ km}}\right)^2 + 1031.72 \times \left(\frac{x}{750\text{ km}}\right)^4 - 151.72 \times \left(\frac{x}{750\text{ km}}\right)^6\right] \text{m}, \tag{10}$$

as shown in Figure 3 (these qualitative features are the sole reason for our choice of $b(x)$). The physical parameters used are given in Table 1. To illustrate the effect of changes in physical parameters, we vary the viscosity coefficient $\bar{A}$ in steps, changing its value once the ice sheet has relaxed to a steady state. The values used for $\bar{A}$ are given in Table 2.

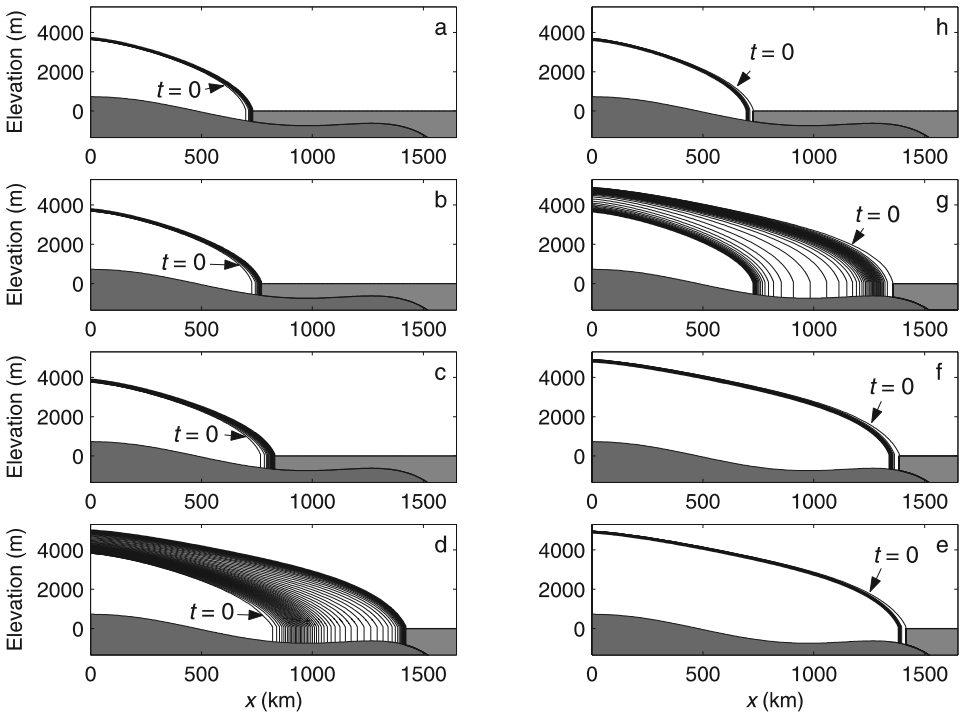

Figure 3. (a–h) Evolution of an ice sheet as $\bar{A}$ is changed stepwise (see Table 2). Ocean is shown in light gray, bedrock in dark gray. Ice sheet surfaces are shown as thin lines at time steps of 500 years, and final shape is shown as a thick line; $t = 0$ indicates initial conditions for each simulation. For each simulation (Figures 3b–3g), the final shape in the previous simulation was used as the initial condition. The initial shape for simulation a is a steady state for $\bar{A} = 4.23 \times 10^{-25}$ s^{-1} Pa^{-3} (which is the final state in Figure 3g). As described in the main text, the entire figure represents a hysteresis loop, with irreversible transitions occurring in Figures 3d and 3g.

[31] As $\bar{A}$ decreases (because of decreases in ice temperature), the steady ice sheet profiles grow from an initial grounding line position at the head of the overdeepening (Figures 3a–3c). Eventually, the grounding line reaches the deepest point of the overdeepening, and subsequently grows until the grounding line moves beyond the sill onto the continental shelf edge (Figure 3d). No steady states appear with the grounding line on the reverse slope of the overdeepening, in agreement with the marine ice sheet instability hypothesis. If $\bar{A}$ is subsequently increased again, the grounding line retreats back up the continental shelf edge, but the ice sheet does not return to the previous steady state profiles attained for the same value of $\bar{A}$ (Figures 3e–3f). Only once $\bar{A}$ is decreased sufficiently so the grounding line reaches the sill does the ice sheet return to its original shape (Figure 3g). Note that the ice sheet in Figure 3g nearly stabilizes close to the sill, but is not quite able to do so and eventually goes into a rapid retreat across the overdeepening. The computed steady state profiles from each plot are also shown separately in Figure 4.

[32] We observe that ice temperature has a major effect on steady grounding line positions, and that hysteresis is possible under variations in temperature. However, can these observations be interpreted more broadly? Do changes in other parameters have a similar effect?

[33] Direct numerical computation is a powerful tool in understanding marine ice sheet dynamics. However, it is also limited because the qualitative insight it provides is limited by the parameter space that can be sampled.

[34] In order to interpret our numerical results in greater generality, we turn to a simpler model based on a boundary layer analysis of the full model. The next two subsections lay out the simpler model, while results are presented in sections 3.3 and 3.4.

3.1. Simpler Theory: Results From Boundary Layer Analysis

[35] Longitudinal stress is retained in the momentum equation (2) for grounded ice only because it must play an important role in force balance in the transition zone close to the grounding line. In the interior of the ice sheet, longitudinal stress is negligible. This observation is the basis of a boundary layer analysis that produces a much simpler mathematical model for the ice sheet. Briefly, the boundary layer analysis decomposes the ice flow problem into two parts, one that describes the flow of ice in the interior of the ice sheet and one for the transition zone.

Table 1. List of the Parameter Values Used[a]

Parameter	Value
ρ_i	900 kg m^{-3}
ρ_w	1000 kg m^{-3}
g	9.8 m s^{-2}
n	3
m	1/3
C	7.624×10^6 Pa m$^{-1/3}$ $s^{1/3}$
a	0.3 m a^{-1}

[a]Values for $\bar{A}$ are given in Table 2. With the chosen value of C, a basal shear stress of 80 kPa corresponds to a sliding velocity of about 35 m a^{-1}.

Table 2. Values of $\bar{A}$ Used in the Calculations Displayed in Figures 3 and 4 and the Ice Temperatures T to Which They Would Correspond If Ice Temperature Were Uniform[a]

Simulation	T, °C	$\bar{A}$, s^{-1} Pa^{-3}
h	−12	4.227×10^{-25}
a, g	−17	2.478×10^{-25}
b, f	−22	1.370×10^{-25}
c, e	−27	7.433×10^{-26}
d	−32	3.935×10^{-26}

[a]Calculations are based on interpolating data from *Paterson* [1994, chapter 5]. Obviously, rapid basal sliding requires temperate basal ice, and the temperature distribution cannot be uniform. Simulation a was started with a steady state profile obtained for $\bar{A} = 4.337 \times 10^{-25}$ s^{-1} Pa^{-3}.

These two ice flow problems are then spliced together using the procedure of asymptotic matching, and details of the analysis can be found in work by *Schoof* [2007]. A related analysis for steady ice sheets that do not slide and which have constant viscosity was previously developed by *Chugunov and Wilchinsky* [1996].

[36] The resulting model for the interior of the ice sheet is simple. Ignoring the longitudinal stress term allows velocity to be calculated in terms of the driving stress:

$$u = -\left(\frac{\rho_i g}{C}\right)^{\frac{1}{m}} h^{\frac{1}{m}} \left|\frac{\partial(h-b)}{\partial x}\right|^{\frac{1}{m}-1} \frac{\partial(h-b)}{\partial x}. \tag{11}$$

Hence ice flux is

$$q = uh = -\left(\frac{\rho_i g}{C}\right)^{\frac{1}{m}} h^{1+\frac{1}{m}} \left|\frac{\partial(h-b)}{\partial x}\right|^{\frac{1}{m}-1} \frac{\partial(h-b)}{\partial x}. \tag{12}$$

Combined with mass conservation, equation (1), this gives a diffusion equation for ice thickness h:

$$\frac{\partial h}{\partial t} + \frac{\partial q}{\partial x} = \frac{\partial h}{\partial t} - \frac{\partial}{\partial x}\left[\left(\frac{\rho_i g}{C}\right)^{\frac{1}{m}} h^{1+\frac{1}{m}} \left|\frac{\partial(h-b)}{\partial x}\right|^{\frac{1}{m}-1} \frac{\partial(h-b)}{\partial x}\right] = a. \tag{13}$$

This can be recognized as a "shallow ice"-type model in which all flux is caused by sliding rather than shearing.

[37] The transition zone problem that couples the interior of the ice sheet with the ice shelf through the boundary conditions (6) and (9) is more complicated. However, when spliced together with the interior flow, it allows sheet-shelf coupling to be represented simply as boundary conditions that apply to the field equation (13) at the grounding line. These boundary conditions can be thought of as "parameterizing" ice flow across the narrow transition zone in a systematic way, rather than resolving it. A derivation of the boundary condition and details of the transition zone structure are given by *Schoof* [2007].

[38] There are two sets of grounding line boundary conditions, corresponding to different parametric regimes. One applies when longitudinal stresses in the grounded ice sheet as a whole are moderately large, accounting for around 5–10% of the driving stress everywhere (rather than just being important at the grounding line). This corresponds to relatively cold ice ($\bar{A}$ small), fast sliding (C small) and an ice sheet of moderate width. Then the boundary condition is a prescription for grounding line migration in terms of local bed and ice geometry at $x = x_g$ [*Schoof*, 2007, Appendix A]:

$$\left(\frac{\rho_w}{\rho_i}\frac{\partial b}{\partial x} - \frac{\partial h}{\partial x}\right)\frac{dx_g}{dt} = -\frac{\bar{A}}{4^n}(\rho_i g)^n (1-\rho_i/\rho_w)^n h^{n+1} + a + \left(\frac{\rho_i g}{C}\right)^{\frac{1}{m}} h^{\frac{1}{m}} \left|\frac{\partial h}{\partial x} - \frac{\partial b}{\partial x}\right|^{\frac{1}{m}-1} \cdot \left(\frac{\partial h}{\partial x} - \frac{\partial b}{\partial x}\right)\frac{\partial h}{\partial x}. \tag{14}$$

This is combined with (6):

$$h = \frac{\rho_w}{\rho_i} b. \tag{15}$$

We will refer to these boundary conditions combined with the evolution equation (13) as model A.

[39] The other possible set of boundary conditions applies when longitudinal stresses in the grounded sheet away from the grounding line are small. Physically, this alternative boundary condition is a flux condition which applies if ice is not too cold, sliding is slow, or the ice sheet is wide. To a good approximation [*Schoof*, 2007, section 3.3],

$$q(x_g) = \left(\frac{\bar{A}(\rho_i g)^{n+1}(1-\rho_i/\rho_w)^n}{4^n C}\right)^{\frac{1}{m+1}} \left[h(x_g)\right]^{\frac{m+n+3}{m+1}}, \tag{16}$$

at $x = x_g$, which we combine with the flotation equation (15). The boundary conditions (16) and (15) together with equation (13) will be referred to as model B.

[40] Equation (16) is exactly the type of result required to confirm the marine ice sheet instability: it predicts that ice flux increases with ice thickness (or equivalently, with depth to the seafloor). In fact, the dependence of outflow q on ice

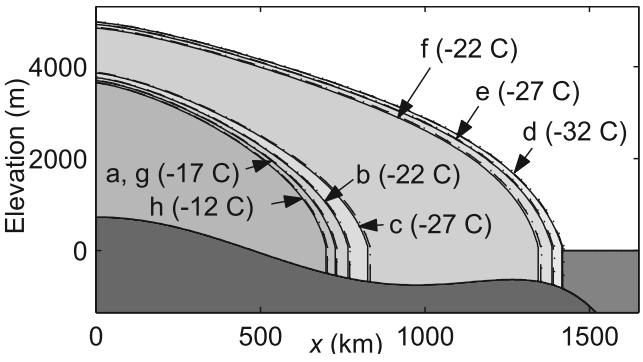

Figure 4. Steady state configurations as computed in Figure 3, with the same labeling a–h. Temperatures in parentheses are those corresponding to the value of $\bar{A}$ as indicated in Table 2. Where more than one steady state corresponds to a given $\bar{A}$, both steady profiles have the same shading. Also shown are the corresponding steady surface profiles computed from boundary layer model A (dashed lines) and model B (dotted lines). These are virtually indistinguishable from the full model results (solid lines), indicating very good agreement.

thickness h at the grounding line is quite sensitive. With $n = 3$ and $m = 1/n$, the exponent is $(m + n + 3)/(m + 1) = 19/4 \approx 5$.

[41] In both models, A and B, the boundary condition at the center of the ice sheet is that surface slope vanishes:

$$\frac{\partial(h-b)}{\partial x} = 0 \qquad \text{at} \qquad x = 0. \tag{17}$$

[42] In summary, boundary layer theory produces two competing results, the more complicated equation (14) and the simple flux prescription (16). The latter (model B) can be interpreted straightforwardly in terms of marine ice sheet instability, while the former (model A) lacks such a clear interpretation.

[43] Incidentally, a flux relation similar to (16) can be constructed from equations (3), (23) and (24) of *Weertman* [1974], though he does not state this explicitly, and the precise form of his flux relation differs from ours. Similarly, equation (A11) of *Thomas and Bentley* [1978] is similar to our equation (14), though formulated by these authors as a global mass balance relation rather than as a boundary condition. The novelty here is that we are able to verify our boundary conditions numerically, and that they arise directly from a boundary layer analysis as described by *Schoof* [2007] and do not require ad hoc approximations in their derivation.

[44] *Chugunov and Wilchinsky* [1996] have previously used boundary layer theory to establish a set of boundary conditions similar to model B for a steady state ice sheet which does not slide and which has constant viscosity ($n = 1$). By contrast with the model used here (a dynamic, rapidly sliding ice sheet with a general Glen's law rheology), their physical setup lends itself less to direct numerical verification because the effect of vertical shearing on the velocity field must be resolved, and a depth-integrated approach is not possible.

[45] Our next tasks are the following: first, we study the accuracy and the ranges of validity of the two sets of boundary layer results, by comparing results based on models A and B with results obtained from the full model consisting of (1), (2), (3), (6) and (9). Second, we use our boundary layer results to study how steady state profiles depend on physical parameters, and what the stability properties of the steady state profiles are. We consider next how to compute these steady states. One of the great advantages of the simplified models (consisting of equation (13) with either model A or model B boundary conditions) is that steady profiles can be predicted semi-analytically.

3.2. Steady Profiles: Simple Calculation

[46] In steady state, equation (13) becomes

$$\frac{\partial q}{\partial x} = a, \tag{18}$$

where the ice flux is given by equation (12). Suppose for simplicity that accumulation rate a is constant. With zero flux at the ice sheet center, we can integrate to find

$$q = ax. \tag{19}$$

Flux at position x simply equals net accumulation ax upstream of that point (in the more general case ax here and below must be replaced by $\int_0^x a(x')\,\mathrm{d}x'$).

[47] Next, the steady grounding line positions must be determined. We start with the easier model B. In steady state, outflow must balance net accumulation, and hence

$$ax_g = q_B(x_g) = \left(\frac{\bar{A}(\rho_i g)^{n+1}(1-\rho_i/\rho_w)^n}{4^n C}\right)^{\frac{1}{m+1}} h(x_g)^{\frac{m+n+3}{m+1}}. \tag{20}$$

This equation determines steady grounding line positions implicitly as functions of bed shape $b(x)$, accumulation rate a and material properties. Graphically, steady grounding line positions correspond to the points of intersection of the graphs of net upstream accumulation ax and outflow through the grounding line $q_B(x)$ plotted against x.

[48] An example is given in Figure 5. Importantly, there is a discrete number of points of intersection. This implies that neutral equilibrium is not possible: if the grounding line is perturbed slightly from a steady state position, then it is no longer in steady state and must either grow or shrink.

[49] We consider model A analogously. Putting $\mathrm{d}x_g/\mathrm{d}t = 0$, (14) becomes

$$-\frac{\bar{A}}{4^n}(\rho_i g)^n(1-\rho_i/\rho_w)^n h^{n+1} + a + \left(\frac{\rho_i g}{C}\right)^{\frac{1}{m}} h^{\frac{1}{m}}\left|\frac{\partial h}{\partial x} - \frac{\partial b}{\partial x}\right|^{\frac{1}{m}-1} \cdot \left(\frac{\partial h}{\partial x} - \frac{\partial b}{\partial x}\right)\frac{\partial h}{\partial x} = 0. \tag{21}$$

Using (12), this can be rewritten as

$$a + \frac{q}{h}\left(\frac{\partial b}{\partial x} - \frac{C}{\rho_i g}\frac{|q|^{m-1}q}{h^{m+1}}\right) + \frac{\bar{A}}{4^n}(\rho_i g)^n(1-\rho_i/\rho_w)^n h^{n+1} = 0, \tag{22}$$

where $q = q(x_g)$. Interestingly, this can in turn be rewritten in the form (16) when $a = \partial b/\partial x = 0$, indicating that (16) is in fact a special case of (14): with $a = \partial b/\partial x = 0$ we have

$$-\frac{C}{\rho_i g}\frac{|q|^{m+1}}{h^{m+2}} + \frac{\bar{A}}{4^n}(\rho_i g)^n(1-\rho_i/\rho_w)^n h^{n+1} = 0, \tag{23}$$

from which (16) follows by simple manipulation.

[50] Given a grounding line position x_g, $h = \rho_w\, b/\rho_i$ and $\partial b/\partial x$ in equation (22) are simply ice thickness and bed slope at that position, and the equation can be solved numerically for the steady state grounding line flux q. Recognizing that q is then a function of grounding line position, we express this flux as $q = q_A(x_g)$. In order for the ice sheet to be steady, this flux must also equal $q = ax_g$. Grounding line position x_g therefore satisfies

$$ax_g = q_A(x_g). \tag{24}$$

In other words, equation (24) has the same form as (20), but $q_A(x)$ cannot be evaluated explicitly in terms of bed geometry. Nonetheless, the position of steady grounding lines x_g can again be visualized as the intersection between net upstream accumulation ax and steady state outflow

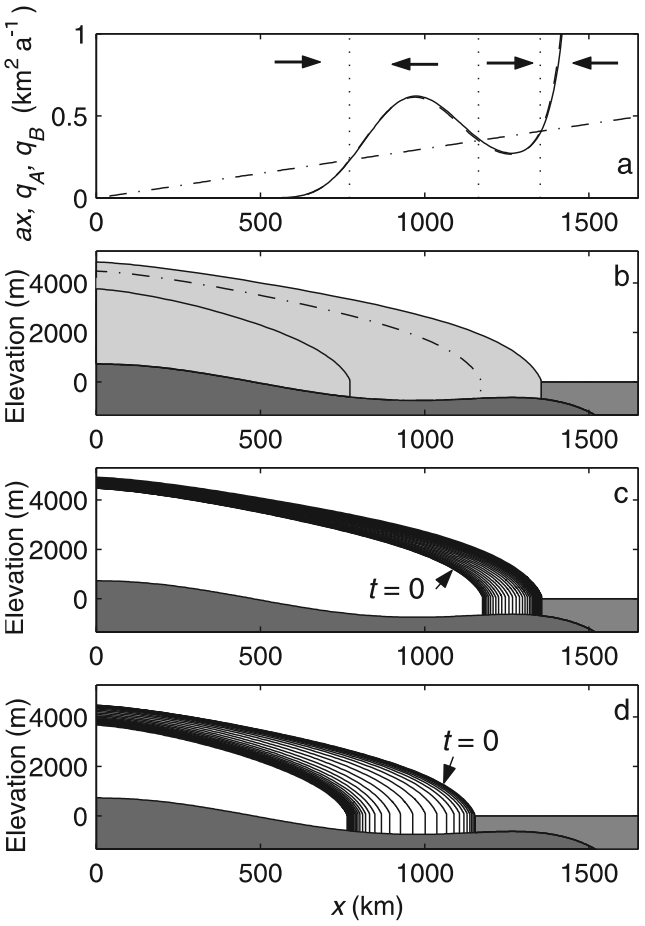

Figure 5. (a) Plot of ax, $q_A(x)$ and $q_B(x)$ against x as dash-dotted, dashed, and solid lines, respectively. Parameter values are those in Table 1 with $\bar{A} = 1.37 \times 10^{-25}$ Pa^{-3} s^{-1}. Vertical dotted lines indicate steady grounding lines for model B (points of intersection of ax and $q_B(x)$), while the arrows indicate likely directions of grounding line migration between these steady states: shrinkage where outflow $q_B(x)$ exceeds ax and growth elsewhere. (b) Corresponding steady surface profiles computed from model B. The dashed profile is unstable, as confirmed by computations with (c and d) the full model; $t = 0$ indicates initial shapes, chosen close to the unstable steady profile in Figure 5b. Time steps shown are 500 years.

$q_A(x)$, plotted as functions of x. In Figure 5, the curve $q_A(x)$ is plotted alongside $q_B(x)$. Again, there are a discrete number of steady positions, and neutral equilibrium is not possible in either model A or B. The $q_A(x)$ curves is also barely distinguishable from the $q_B(x)$ curve, as was already suggested by the virtually identical model A and B profiles in Figure 4.

[51] Once the grounding line position x_g is known, the surface profiles can be found by rewriting (19):

$$\frac{\partial h}{\partial x} = \frac{\partial b}{\partial x} - \frac{C}{\rho_i g}\frac{|q|^{m-1}q}{h^{m+1}} \qquad \text{where} \quad q = ax. \tag{25}$$

This differential equation must then be integrated with an ordinary differential equation solver from x_g, where $h = (\rho_w/\rho_i)b$.

3.3. Comparison: Full Model Versus Boundary Layer Theory Results

[52] In Figure 4, the steady ice sheet profiles predicted by models A and B are plotted alongside the solutions of the full model (equations (1), (2), (3), (6) and (9)) for the same model parameters. All three models are in very close agreement for all parameter values chosen (in particular, for high and low values of $\bar{A}$), and the close-ups in Figure 6 are required to see the difference between the profiles. (Models A and B are, of course, only approximations of the full model, and exact agreement cannot be expected.)

[53] Models A and B consistently overestimate the size of the steady state ice sheet, but the error in width is always less than 20 km, and the error in ice thickness does not exceed 150 m. Model A performs somewhat better than model B, though not significantly so, and the error compared with the full model is small in both cases. (The close agreement between model A and B steady states can probably be traced to the observation leading up to equation (23), that model B is a special case of model A: the extra terms contained in equation (22) compared with (23) presumably represent only small corrections. More important, however, is that they both closely reproduce the full model steady states.)

[54] The agreement between the models can be seen either as a verification of our numerical solution of the full model or as vindication of the boundary layer theory. Either way, it suggests that we have obtained reliable results, and that steady state results calculated from boundary layer theory can be used to benchmark numerical solutions of the full marine ice sheet model. Moreover, we see that models A and B agree closely, and that it may suffice to use the simpler model B for qualitative work.

[55] To validate our results further, we compare the dynamic models A and B with the dynamic full model. We recompute the transient shown in Figure 3g using models A and B, and compare these results with results of the full model. The numerical scheme for solving model B is described in detail in Appendix A, while model A is discretized analogously. As a proxy for dynamical behavior, we plot grounding line position as a function of time in Figure 7.

[56] Discrepancies between the models become more apparent here, as the transients differ much more discernably from one another than the final steady states. Model A performs noticeably better than model B in reproducing the

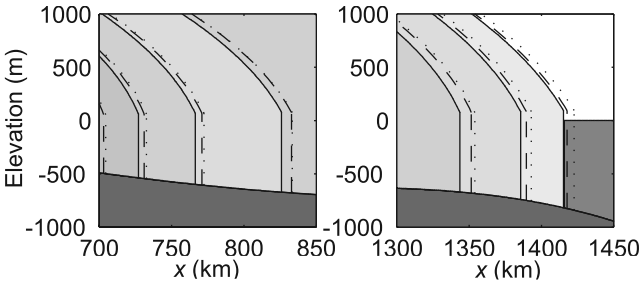

Figure 6. Close-up of Figure 4 to show the differences between boundary layer and full model results. Solid lines are full model results, dashed line is model A, and dotted line is model B.

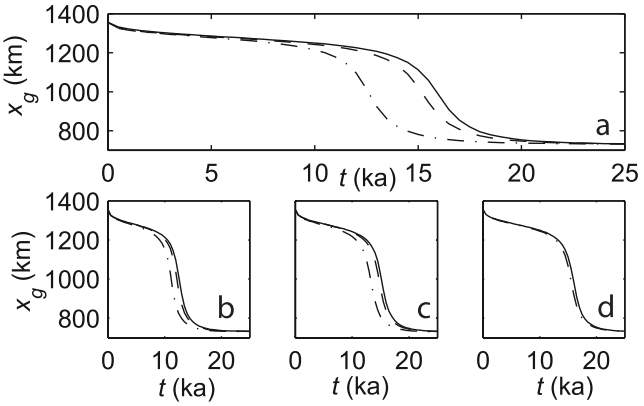

Figure 7. (a) Plot of $x_g(t)$ for the transient shown in Figure 3g, for the full model (solid line), model A (dashed line), and model B (dash-dotted line). Grid parameters (see Appendix A) are $N_1 = N_2 = 4000$ with $D = 0.0274$. (b–d) Transients computed with models A and B and the full model, respectively, with coarser resolutions: $N_1 = N_2 = 4000$ (solid line), $N_1 = N_2 = 2000$ (dashed line), and $N_1 = N_2 = 1000$ (dash-dotted line).

transient behavior. The difference between the solutions lies mostly in the time taken for the grounding line to retreat across the shallow sill. This takes somewhat longer (~1 ka) in the full model than in model A, which in turn retreats considerably more slowly than model B (~4 ka). Once the rapid retreat across the overdeepening has begun, corresponding to the steep part of the $x_g(t)$ curve, all three models behave similarly.

[57] Some of these discrepancies probably arise because the initial configuration of the ice sheet lies close to a bifurcation. This bifurcation is the "tipping point" at which the steady grounding line on the continental shelf disappears as $\bar{A}$ is increased (see section 3.4). Close to this bifurcation, slight differences in initial conditions due to changes in the discretization could become amplified, and this probably results in at least part of the observed discrepancies.

[58] However, it is clear that model A reproduces the dynamic full model results better than model B. As we have seen above, the approximations made in obtaining model B from the steady state version of model A introduces only minor errors (see the derivation of equation (23)). This is clearly not the case in dynamic calculations, and can be attributed to the time derivative term dx_g/dt in (14). This term only affects model A results in the dynamic case, and has no equivalent in model B. Formal error estimates given by *Schoof* [2007, section 3.3, equation (3.37)] confirm this, showing that the time derivative term is a lower-order correction to (16) than the other terms retained in (14).

[59] To some extent, the discrepancies between model A, model B and full model results may also be due to numerical errors in the finite difference schemes. Figures 7b–7d shows numerical solutions computed with high grid resolutions and grid refinement near the boundary alongside results for coarser grids. Changing the grid spacing has a discernable effect on the computed transient behavior, which is indicative of numerical errors. As indicated, these errors may however be exacerbated by the initial proximity to a bifurcation.

[60] Interestingly, the calculated final steady states in Figure 7 do not depend significantly on grid spacing, merely the transients do. This is also true of the entire ice sheet profiles, not just the grounding line positions plotted here. The computed transients are also much more robust to changes in time steps than to changes in grid spacing, although we have not plotted these calculations here. These results suggest a need for significant grid refinement in dynamical calculations.

3.4. Steady Profiles: Stability, Parameter Dependence, and Hysteresis

[61] The results in Figures 3 and 4 have already indicated the possibility of multiple steady states, and hence of hysteresis under parameter forcings. The existence of multiple steady states can be visualized easily using the boundary layer results, as is shown in Figure 5: here, the curves $q_B(x)$ (or $q_A(x)$) and ax intersect more than once, and predict the two steady states shown in Figure 4 for $\bar{A} = 1.37 \times 10^{-25}$ s^{-1} Pa^{-3}.

[62] Importantly, there is also a third point of intersection in Figure 5a, corresponding to a steady profile with its grounding line position on the reverse slope of the overdeepening, as shown as a dash-dotted outline in Figure 5b. This steady profile is not reproduced in Figure 4. The arrows in Figure 5 serve as a simple explanation: if the grounding line is moved slightly to the right of the steady

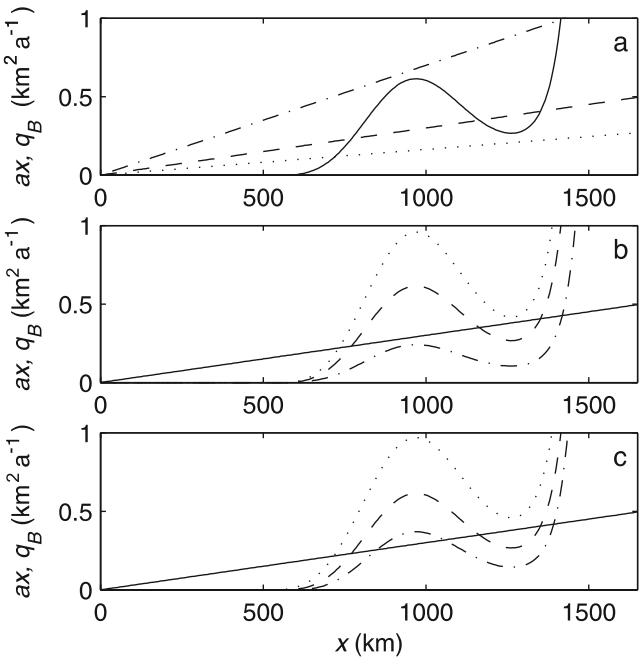

Figure 8. Plots of ax and q_B against x for the bed described in (10). Parameters are those in Table 1, except where indicated otherwise: (a) $\bar{A} = 1.37 \times 10^{-25}$ Pa^{-3} s^{-1} and $a = 0.3$ m a^{-1} (dashed line), 0.7 m a^{-1} (dash-dotted line) and 0.15 m a^{-1} (dotted line); (b) $a = 0.3$ m a^{-1} and $\bar{A} = 1.37 \times 10^{-26}$ Pa^{-3} s^{-1} (dashed line), 3.94×10^{-26} Pa^{-3} s^{-1} (dash-dotted line), and 2.48×10^{-25} Pa^{-3} s^{-1} (dotted line); (c) a, C, and $\bar{A}$ are the same as in Figure 5, and $\Delta h_w = 0$ (dashed line), 75 m (dotted line), and −75 m (dash-dotted line).

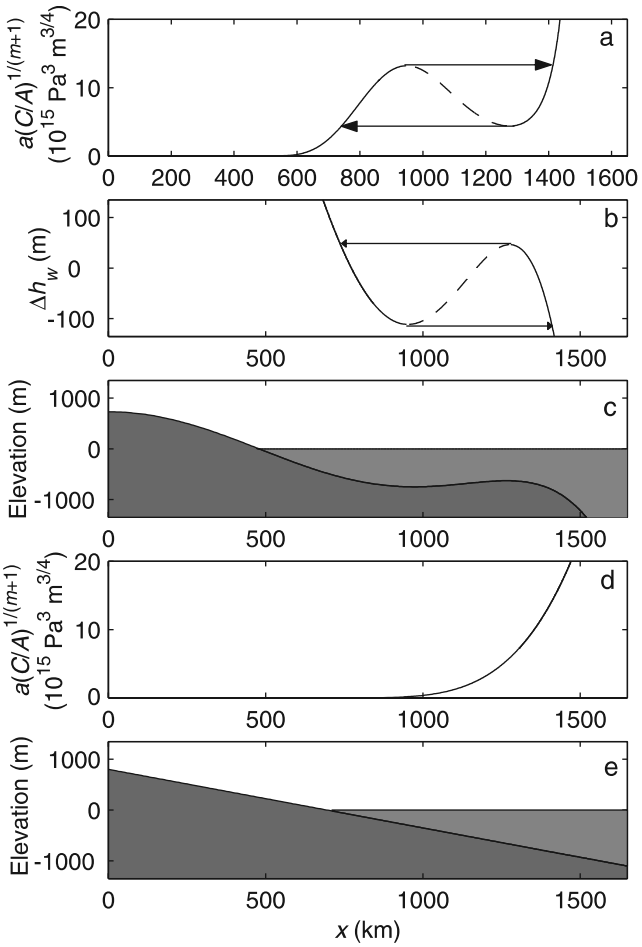

Figure 9. (a and b) Grounding line position as a function of physical parameters. In Figure 9a, parameters are as in Table 2, but C, $\bar{A}$, and a can vary. In Figure 9b, parameters are as in Table 1 and $\bar{A} = 1.37 \times 10^{-25}$ Pa^{-3} s^{-1}, while sea level Δh_w can vary. (c) Bed shape as defined in equation (10). (d) Plot analogous to Figure 9a but computed for the bed shape in equation (27). (e) Bed shape as defined in equation (27). Arrows in Figures 9a and 9b indicate possible hysteresis loops.

position, net accumulation ax exceeds outflow $q_B(x)$ (or $q_A(x)$) and the ice sheet will continue to grow. The reverse is true if the grounding line position is perturbed slightly to the left. This is of course nothing more than the marine ice sheet instability mechanism, and shows that the dashed profile in Figure 5b is unstable. By contrast, the other two profiles (solid lines in Figure 5b) are stable: a slight increase in size leads to negative mass balance and hence shrinkage, while a slight decrease in ice sheet size leads to positive mass balance, and hence to growth.

[63] These stability properties are verified using the full model: Figures 5c and 5d show simulations started with initial conditions slightly smaller and larger than the suspected unstable steady profile, and as expected, these evolve to reproduce the other two, stable surface profiles. Simulations with the dynamic models A and B produced the same qualitative results, which we have not plotted here. An animation of these stability properties (Animation 1) is also included.[1]

[64] Next, we go on to consider how steady grounding line positions depend on the material parameters $\bar{A}$ and C representing (mean) ice temperature and bed friction, as well as the climatic forcings represented by accumulation rate a and by changes in sea level. We restrict ourselves to model B, as this furnishes the simplest description of steady grounding lines through equation (20) and performs well in computing steady states. We also continue to use the bed shape prescribed in equation (10) to illustrate the behavior of an ice sheet with an overdeepening.

[65] Under changes in physical parameters, Figure 5 generalizes to the intersection between families of curves representing $q_B(x)$ and ax, as shown in Figure 8. We are interested in conditions that favor multiple points of intersection. For a bed shape such as that used in Figure 3 (given by equation (10)), this generally implies one stable steady grounding line on the downward sloping part of the overdeepening, and another close to the continental shelf edge.

[66] For this bed shape, the flux curve $q_B(x)$ will generically have the shape shown in Figure 5, with the first peak corresponding to the lowest point of the overdeepening, the trough corresponding to the shallow sill, and the final rising limb corresponding to the dropoff of the continental shelf. This is the case because $q_B(x)$ increases monotonically with $h(x)$. Merely the amplitude of variations on the curve is affected by parameter changes. The curve will move up if $\bar{A}$ is large: ice flux through the grounding line increases as temperature increases, because the imposed stress in (9) at the grounding line will lead to a larger strain rate. Similarly, the flux curve will move up if the friction parameter C decreases. Flux increases if the bed is more slippery.

[67] Conversely, the straight line ax slopes up more steeply for larger accumulation rates: more ice must flow out through the grounding line if accumulation rates are high (and if the ice sheet is wide). Intersections between the ax and $q_B(x)$ curves on the final rising limb of the $q_B(x)$ curve are more likely to occur when accumulation rates are large, when ice is cold and bed friction is high, while points of intersection to the left of the first maximum of the $q_B(x)$ curve are favored by low accumulation rates, high temperatures and high sliding rates. In between these regimes, multiple steady states are possible (Figure 8).

[68] Figure 9a shows steady grounding line positions as functions of $a(C/\bar{A})^{1/(m+1)}$. For a fixed bed shape, this is the single parameter through which a, C and $\bar{A}$ enter into the steady state grounding line problem (20), which can be written as

$$\frac{aC^{1/(m+1)}}{\bar{A}^{1/(m+1)}} x_g = \left(\frac{(\rho_i g)^{n+1} (1 - \rho_i/\rho_w)^n}{4^n} \right)^{\frac{1}{m+1}} h(x_g)^{\frac{m+n+3}{m+1}}. \quad (26)$$

There are two stable branches in this plot (shown as solid lines), connected by an unstable one (shown as a dashed line). An "unstable branch" is simply a part of the curve corresponding to unstable profiles that will not be attained in practice.

[69] The stable branch with wider ice sheets is favored by larger $a(C/\bar{A})^{1/(m+1)}$, while the branch with smaller ice sheets

[1] Animations are available in the HTML.

is favored by smaller $a(C/\bar{A})^{1/(m+1)}$. Hysteresis under parameter changes is possible as a result of switches between the two branches. These switches occur when the parameter $a(C/\bar{A})^{1/(m+1)}$ reaches the "tipping points" (or more appropriately, bifurcation points) indicated by arrows. Of course, the presence of an overdeepening is essential for the presence of two steady state branches and hence hysteresis. To reinforce this point, we plot in Figure 9d steady grounding line positions against $a(C/\bar{A})^{1/(m+1)}$ for the simple, downward sloping bed,

$$b(x) = -\left(720 - 778.5 \times \frac{x}{750\ \mathrm{km}}\right)\mathrm{m}. \tag{27}$$

Clearly, there is then a single stable grounding line position for every $a(C/\bar{A})^{1/(m+1)}$, and no hysteresis.

[70] Next, we consider the effect of sea level changes. As grounding line ice flux depends on ice thickness, changes in sea level directly affect outflow for a given grounding line position. Let $b(x)$ describe the bed shape for a reference sea level, and increase sea level by an amount Δh_w. Then ice thickness at grounding line position x_g changes from $\rho_w b(x_g)/\rho_i$ to $\rho_w[b(x_g) + \Delta h_w]/\rho_i$. $q_B(x_g)$ changes to

$$q_B(x_g) = \left(\frac{\bar{A}(\rho_i g)^{n+1}(1-\rho_i/\rho_w)^n}{4^n C}\right)^{\frac{1}{m+1}} \cdot \left[\frac{\rho_w\left(b(x_g) + \Delta h_w\right)}{\rho_i}\right]^{\frac{m+n+3}{m+1}}. \tag{28}$$

An increase in sea level increases grounding line flux, moving the $q_B(x_g)$ curve up. The effect on steady states is therefore similar to an increase in $\bar{A}$ or decrease in C. Because $q_B(x_g)$ is very sensitive to ice thickness at the grounding line through the exponent $(m + n + 3)/(m + 1) \approx 5$, $q_B(x_g)$ is similarly sensitive to changes in sea level.

[71] In Figure 9b, we show how steady state grounding line positions depend on Δh_w for the bed given by equation (10). Again, two stable branches appear on the curve, and hysteresis is possible under variations in sea level. The branch corresponding to large ice sheets is favored by lower sea levels (negative Δh_w), while the smaller branch is favored by higher sea levels (positive Δh_w). An animation of hysteresis under changes in Δh_w (Animation 2) is also provided.

4. Discussion

[72] Marine ice sheets are unique because their dynamics are strongly controlled by outflow of ice across the grounding line, whereas there is no ice flux through the margin of a land-based ice sheet. Changes in outflow can lead to drastic changes and even complete collapse in an ice sheet even in the absence of melting (which is often regarded as a key component in deglaciation).

[73] Physically, outflow is controlled by a combination of longitudinal and vertical shear stresses in the sheet-shelf transition zone, where both of these stress components play a leading-order role. Importantly, this is true even if longitudinal stresses are transmitted only a short distance into the grounded sheet.

[74] Our results have shown that the shape of the bed controls the outflow of ice along with ice viscosity and the slipperiness of the bed. Ice flux out of the grounded ice sheet in a two- dimensional sheet-shelf system increases when the bed at the grounding line is deeper below sea level, or when ice viscosity is lower or the bed is more slippery. The dependence on the depth of the bed below sea level is particulary sensitive; we find a power law with an exponent close to 5.

[75] In the remainder of section 4 we discuss the implications of our results, considering in turn past and future ice sheet dynamics, physical effects not covered by our model and comparisons with other attempts to model marine ice sheet dynamics. The subsections below can be read independently of one another.

4.1. Marine Ice Sheets Past and Future: Role of Hysteresis

[76] With respect to the only marine ice sheet presently in existence, the West Antarctic ice sheet, the most important result in this paper is that marine ice sheets with overdeepenings can undergo hysteresis under changes in internal physical parameters (viscosity, slipperiness) or under changes in external forcing, notably through changes in accumulation rate or sea levels (Figure 9). A similar hysteresis mechanism under accumulation rate changes has also been considered for tidewater glaciers in the much simpler models of *Oerlemans and Nick* [2005, 2006], but without a detailed consideration of the physics involved.

[77] The central parts of West Antarctica are significantly overdeepened compared with the continental shelf edge. Observations have shown that the grounding line in West Antarctica has retreated up to 1000 km since the Last Glacial Maximum from a location near the continental shelf edge, and may continue to do so [*Conway et al.*, 1999]. A simple explanation for this phenomenon furnished by our theory is that, during glacial periods, the ice sheet undergoes hysteretic transitions from a small configuration centered around the Ellsworth mountains and Marie Byrd Land (possibly stabilized by the Ross and Ronne-Flichner ice shelves, see below) to a large configuration extending to the continental shelf edge, and that the reverse transition occurs at deglaciation. *Conway et al.* [1999] suggested sea level rise due to ice sheet melting in the Northern Hemisphere as a possible trigger for the abrupt onset of grounding line retreat after the Last Glacial Maximum, and our results confirm this teleconnection between ice sheets as a strong possibility.

[78] Another interesting aspect of the hysteretic behavior of overdeepened ice sheets is that an ice sheet can easily form its own overdeepening over time through isostatic depression and subglacial erosion, and one can envision that an initially stable ice sheet may eventually develop hysteretic behavior after carving out such an overdeepening.

[79] With respect to the present-day evolution of ice sheets, the overdeepenings of Thwaites and Pine Island glaciers [e.g., *Vaughan et al.*, 2006] are obvious locations in which irreversible grounding line retreat could be triggered. Moreover, the recent synchronous retreat of fjord-bound outlet glaciers in Greenland [*Howat et al.*, 2005; *Luckman et al.*, 2006] suggests that similar, abrupt and potentially irreversible retreat may also be possible in outlet glaciers in overdeepened channels, though it is still unclear precisely

what has triggered the glacier retreat in Greenland. (In terms of our results, a decrease in coastal accumulation rates under a warming climate seems the most obvious candidate [see also *Oerlemans and Nick*, 2005, 2006], but the direct impact of warmer ocean waters discussed in section 4.3.2 or enhanced bed-slipperiness due to surface melt water input are equally plausible).

[80] The relationship between marine ice sheet hysteresis and Heinrich events is more difficult to determine. Heinrich events are episodic discharges of ice-rafted debris from the northern hemisphere ice sheets during the last glacial period, which have generally been associated with large discharges of sediment-laden icebergs from an ice stream situated in the Hudson Strait sector of the Laurentide ice sheet [*Hemming*, 2004]. Various glaciological mechanisms for Heinrich events have been proposed, among them thermally regulated surges of the Hudson Strait ice stream [*MacAyeal*, 1993] and catastrophic breakup of an ice shelf fringing the mouth of Hudson Strait [*Hulbe et al.*, 2004]. The possibility of a marine ice sheet instability mechanism was also raised by *Clarke et al.* [1999], though phrased by these authors in terms of the dynamics of tidewater glaciers.

[81] In brief, the mouth of Hudson Strait has an overdeepening that could give rise to the type of hysteretic behavior predicted by our model. A possible interpretation of Heinrich events is that the discharge of sediment-laden icebergs occurred as a result of an abrupt and irreversible retreat of the grounding across this overdeepening, as shown in Figure 3g. Importantly, such a retreat could be triggered by external climatic variations, for instance if there were a drop in accumulation rate a due to low precipitation levels at the coldest point in the Bond cycle, or a rise in sea levels as envisaged by *Flückiger et al.* [2006]. Equally, a retreat of this type could occur because of internal changes in the ice sheet increasing basal slipperiness (decreasing C in our model), as envisaged by the binge-purge oscillator of *MacAyeal* [1993]. The precise interplay between climatic forcing, internal thermomechanical changes and grounding line dynamics will need to be taken up by future work, and points to the need for a better representation of ice stream dynamics in marine ice sheet models.

4.2. Missing Piece: Buttressing

[82] We now turn to the main limitation of our model, namely that it describes only a two-dimensional ice sheet. This restriction allows us to decouple the evolution of the shelf from the problem of grounded ice flow through the stress boundary condition (9), which in turn is useful in validating numerical results: results obtained from a coupled sheet-shelf model must agree with those obtained from solving a model for the grounded sheet only. Moreover, changes to a two-dimensional ice shelf, for instance through basal melting, do not affect the grounded sheet. However, we reiterate that these observations only hold if the shelf is freely floating and two dimensional and has a finite extent.

[83] In three dimensions, the explicit integration of the momentum conservation equation to produce the boundary condition equation (9) is no longer possible. In general, if the ice shelf is confined to an embayment or makes contact with the seafloor to form ice rumples, grounding line stresses are likely to be below the value in (9). To see the significance this buttressing effect may have, note that a reduction in grounding line stress by a factor $\theta < 1$ compared with equation (9) changes the flux prescription (16) to

$$q_B(x_g) = \left(\frac{\bar{A}(\rho_i g)^{n+1}(1-\rho_i/\rho_w)^n}{4^n C}\right)^{\frac{1}{m+1}} \theta^{\frac{n}{m+1}} h^{\frac{m+n+3}{m+1}}. \qquad (29)$$

In other words, grounding line flux is about half as sensitive to buttressing as it is to ice thickness h: with $n = 1/m = 3$, we have a power law with exponent 9/4: reduction in stress by a factor of 1/2 reduces flux by a factor of 0.2102.

[84] The removal a buttressing ice shelf can therefore be expected to speed up ice discharge significantly from the glaciers or ice sheet draining into it. This was confirmed observationally by *Rignot et al.* [2004] following the collapse of the Larsen B ice shelf. Of course, the loss of a buttressing ice shelf need not lead to the complete disintegration of a marine ice sheet. If the grounding line is on a downward sloping bed, loss of buttressing may simply lead to a grounding line retreat to a shallower position, where grounding line flux will be reduced again and a new steady state may be attained. Alternatively, retreat could lead to some previously grounded ice becoming afloat, and a buttressing ice shelf could form anew if climatic conditions permit.

[85] Importantly, buttressing cannot simply be parameterized through a correction factor θ as suggested above: the factor θ cannot be treated as given, but must be determined through momentum conservation in the ice shelf [e.g., *Schoof*, 2006], which in turn depends on the evolving three-dimensional geometry of the ice shelf. The development of models for three-dimensional marine ice sheet/ice shelf systems will need to address this issue. Axisymmetric ice sheets form an exception here, as they can be dealt with in a two-dimensional framework.

[86] Our stability and hysteresis results were obtained from a two-dimensional model, and the limitations due to buttressing described above become significant mostly when the grounding line retreats into an embayment and a confined ice shelf develops. In terms of West Antarctica, this is the case during the shrinkage of the ice sheet away from the continental shelf edge, when the large ice shelves in the Ross and Ronne-Filchner embayments form. It is less relevant when the ice sheet is at its maximum extent and any attached ice sheets are likely to be freely spreading. The explanation of the retreat of the ice sheet in terms of the hysteresis curves in Figure 9 therefore remains viable, but it is not clear whether the ice sheet in its current configuration could be stable even with its grounding line on an upward sloping bed, stabilized Ross and Ronne-Filchner ice shelves. Future work will need to take up this issue.

4.3. Effect of Ocean Warming

[87] Recent observations have suggested a direct link between warmer ocean waters in the Amundsen Sea and the accelerated flow of Pine Island Glacier. *Payne et al.* [2004] and *Bindschadler* [2006] have suggested enhanced melting at the base of the Pine Island Glacier ice shelf associated with the so-called ice pump [e.g., *Holland and Jenkins*, 2001] as the likely cause. In detail, they propose that enhanced melting reduces contact between ice and bed,

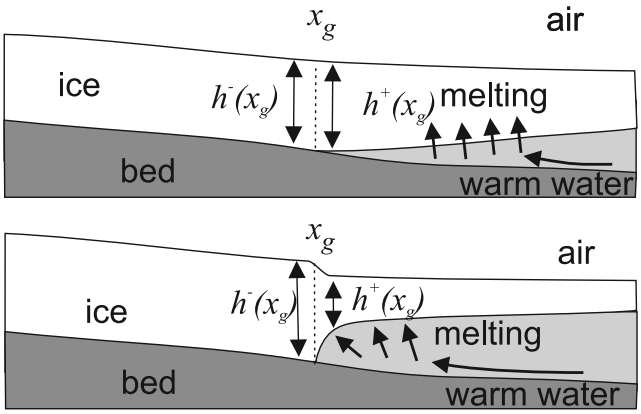

Figure 10. (top) Diagram showing that significant amounts of warm ocean water will not reach the grounding line directly if the shelf bottom slope there is small. (bottom) Diagram showing that strong melting directly at the grounding line is possible if the shelf bottom slope is steep there. In that case, ice thickness near the grounding line on the shelf side (h^+) will generally be less than flotation, and more on the sheet side (h^-), while both will be at flotation if the shelf bottom slope is small (top plot).

and therefore reduces basal friction. This specific mechanism is however questionable.

[88] The enhanced melting presumably happens where the ice is already afloat and therefore not subject to interfacial friction to start with. Unless ocean water can leak upstream of the grounding line (therefore flowing upstream in a subglacial drainage system), it is unclear how basal melting induced by ocean warming can directly lead to reduced basal friction.

[89] We have emphasized that the ice shelf is a passive component in our full model, implying that enhanced melting at the shelf bottom should not affect grounded ice flow. So what causes a link between ocean warming and accelerated flow of grounded ice? How do we need to amend our model to capture this link? There are two plausible explanations, both of which do involve shelf bottom melting. We describe them next.

4.3.1. Reduced Buttressing

[90] The ice shelf of Pine Island Glacier is not two dimensional but confined in a narrow embayment. Changes in ice shelf geometry (and hence in buttressing) will therefore affect longitudinal stresses and hence ice fluxes at the grounding line as discussed in section 4.2 above. As we shall see, enhanced bottom melting can change ice shelf geometry in a way that causes higher ice fluxes at the grounding line.

[91] Melting at the shelf base is concentrated near the grounding line [*Holland*, 2002]. This steepens the shelf near the grounding line, and flattens it away from the grounding line. Hence enhanced bottom melting leads to a greater driving stress in the shelf close to the grounding line. Because of the proximity to the grounding line, longitudinal stresses will support more of this enhanced driving stresses than if it acted further away from the grounding line, in which case drag from the sides of the shelf would be dominant. The increased longitudinal stresses will then cause a larger ice flux across the grounding line as discussed in section 4.2.

[92] Enhanced shelf bottom melting can therefore plausibly reduce the buttressing effect of the shelf sides, by concentrating ice shelf driving stress near the grounding line. To capture this effect in our model, an extension to three dimensions is necessary as discussed in section 4.2 above.

4.3.2. Direct Melting at the Grounding Line

[93] Shelf bottom melting could directly cause a retreat of the grounding line by melting back grounded ice there. For this to happen, the base of the shelf at the grounding line must slope steeply upward, so that warm ocean waters can come into direct contact with grounded ice (see Figure 10). This can lead to faster grounding line retreat and faster grounded ice flow as described below.

[94] We emphasize that this melt-back scenario requires a very steep shelf base near the grounding line. As discussed below, one of its testable implications is that grounded ice thickness at the grounding line should exceed flotation by an appreciable amount. It is unclear whether this is the case at Pine Island Glacier, and reduced ice shelf buttressing (section 4.3.1) may be a stronger contender to explain the acceleration of grounded ice there: reduced buttressing does not require melting and a steep bottom slope at the grounding line itself, but merely enhanced melting near the grounding line.

[95] A near-vertical shelf bottom at the grounding line significantly alters our full model (consisting of equations (1), (2), (3), (6) and (9)). Specifically, ice thickness at the grounding line in the depth-integrated full model can no longer be treated as continuous. This is the case because the depth-integrated model cannot resolve the flow physics associated with steep ice slopes (comparable to 45°), such as locally noncryostatic vertical stresses.

[96] One consequence of discontinuous h is that h on the grounded side of the grounding line need no longer be at flotation, but will generally exceed the flotation thickness by some finite amount, while h on the shelf side will be less than flotation. (Importantly, if ice thickness remains at flotation, then the full model of the present paper with grounding line boundary conditions (6) and (9) still holds at least for a two-dimensional ice sheet, and there is no melt-back effect on the large-scale grounded ice dynamics).

[97] When grounded ice thickness at the grounding line exceeds flotation, the stress condition (9) no longer holds but must be replaced by (see Appendix B)

$$2\bar{A}^{-1/n}h\left|\frac{\partial u}{\partial x}\right|^{1/n-1}\frac{\partial u}{\partial x}=\frac{1}{2}\left(\rho_i g h^2-\rho_w g b^2\right), \qquad (30)$$

where h is grounded ice thickness at the grounding line. If ice thickness is above flotation, then $h > (\rho_w/\rho_i)b$ and so

$$\frac{1}{2}\left(\rho_i g h^2-\rho_w g b^2\right)>\frac{1}{2}\rho_i\left(1-\frac{\rho_i}{\rho_w}\right)g h^2.$$

Hence the stress on the right-hand side of (30) is greater than that predicted by equation (6). This enhanced stress then causes faster ice flow at the grounding line as discussed in section 4.2.

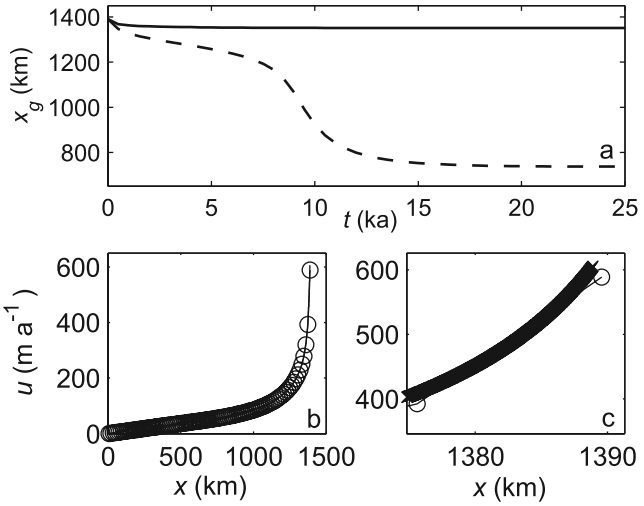

Figure 11. (a) Grounding line position against time for the simulation shown in Figure 3f. Solid line shows solution computed with the numerical method in Appendix A, with $N_1 = N_2 = 1000$, $D = 0.0317$. The dashed line shows the same solution computed with 100 equally spaced grid points. (b) Velocity field at the first time step, with grid points shown as circles for the coarse grid. The sheet-shelf transition zone boundary layer corresponds to the sharp increase in velocity close to the grounding line. (c) Close-up of Figure 11b, with grid points shown as circles for the coarse grid and as crosses for the fine grid. The discrepancies between results can be attributed to underresolution with the coarser grid.

[98] Obviously, coupling with the shelf can also no longer be described by the flotation boundary condition (6). Instead, a rate of grounding line retreat must be specified directly as a result of melting at the grounding line (this prescription would then play a similar role to calving rates in tidewater glacier models [see *van der Veen*, 1996]). We do not consider this problem in detail here.

[99] A boundary layer description for ice flow in the sheet-shelf transition zone for this melt-back scenario remains to be attempted. However, it is clear that it should generate faster rates of grounding line retreat than those computed by the theory in the present paper, as well as faster rates of ice flow near the grounding line.

[100] The possibility of undercutting grounded ice by melting directly at the grounding line is also relevant to tidewater glaciers. These glaciers are similar to the Greenland outlet glaciers mentioned above [*Howat et al.*, 2005; *Luckman et al.*, 2006], which generally lack an ice shelf and consequently interact directly with ocean waters. The basic changes to the full model outlined in this subsection (with the caveat that grounding line retreat is likely to be controlled by direct calving) would also make it applicable to tidewater glacier dynamics, and this represents an obvious avenue for future research [see also *Vieli et al.*, 2001].

4.4. Comparison With Previous Modeling Attempts

[101] We have already touched on some of the technical issues that have beset many efforts to model marine ice sheet dynamics numerically. Drawing these together, a number of observations are especially relevant.

[102] Typically, there are two types of numerical marine ice sheet models, ones that employ the shallow ice approximation, and ones that resolve longitudinal stress throughout the ice sheet (the MGSHXX and MGSTSF models, respectively, of *Vieli and Payne* [2005]). The present paper has shown how the two can be reconciled through boundary layer theory, which allows the localized effect of longitudinal stress near the grounding line to be parameterized in the form of a boundary condition at the grounding line (equation (14) or (16) above). It is in fact this boundary condition through which grounding line flux is determined, and which explains the hysteretic behavior of the ice sheet described above.

[103] The main problem with the shallow ice (MGSHXX) model of *Vieli and Payne* [2005] is that it is missing this additional boundary condition. The same is true of the marine ice sheet model of *Hindmarsh* [1996] and *Hindmarsh and LeMeur* [2001]. Mathematically, their models are incomplete, and a rate of grounding line migration cannot be determined. In technical terms, the MGSHXX model is a parabolic free boundary problem in which only one independent boundary condition, namely on ice thickness, has been specified at the free boundary (i.e., at the grounding line). Generic parabolic free boundary problems, such as the Stefan problem, do however require two boundary conditions at the moving boundary. This additional boundary condition cannot be determined by rewriting the field equation along with the one given boundary condition. This rewriting is precisely what is done in equation (B3) of *Vieli and Payne* [2005] and in equation (4) of *Hindmarsh* [1996], but it does not introduce the additional information required of the second boundary condition into the problem. In that sense the MGSHXX models of *Vieli and Payne* [2005] and *Hindmarsh* [1996] are not well posed. The additional boundary condition must be specified separately, and must be determined by the physics of the sheet-shelf transition zone as described by, e.g., *Chugunov and Wilchinsky* [1996] and *Schoof* [2007]. The present paper has considered equations (14) and (16) as possible forms for this additional boundary condition, both of which give results in good agreement with the full, stress-resolving model. A boundary condition similar to (16) is also included in the simplified ice sheet model of *Oerlemans* [2002].

[104] By contrast, numerical issues encountered with the longitudinal stress-resolving MGSTSF model of *Vieli and Payne* [2005] are likely to arise when the transition zone is underresolved. This was already identified as a potential source of numerical error by *Vieli and Payne* [2005] through grid size sensitivity experiments. To underline the point further, we have recalculated the results shown in Figure 3f, but with an equally spaced grid containing 100 grid points for ice thickness (Figure 11a). It is evident that, while the more highly resolved model settles to a steady state on the sill side of the overdeepening in agreement with the boundary layer results, the more crudely resolved model does not and instead retreats across the overdeepening. Figure 11b indicates why this is the case: the sharp increase in ice velocity near the grounding line is not resolved spatially by the coarser grid, leading to significant model error. It is likely that similar errors occur in the model runs reported by *Vieli and Payne* [2005], which employ relatively coarse grids.

[105] Numerical underresolution may also affect the results of *Pattyn et al.* [2006], who impose a size on the

sheet-shelf transition zone through prescribed spatial variations in basal slipperiness. In their work, neutral equilibrium of steady states is observed when the transition zone is made very small, and our results suggest that this may be an artifact due to numerical underresolution. As we have stressed, longitudinal stress at the grounding line need not propagate far into the ice sheet, but will always play a controlling role in outflow of ice across the grounding line. In a model in which this effect is not parameterized in the form of a boundary condition (i.e., in our full model as opposed to our boundary layer models), it is therefore essential that the zone in which longitudinal stresses are important be resolved. We reiterate that the numerical scheme used in the present paper is specifically designed to do this, on the basis of a grid refinement guided by an a priori estimate of the transition zone width (equation (A9) of Appendix A below) [see also *Schoof*, 2007].

5. Conclusions

[106] In this paper, we have used a combination of numerical and analytical results to confirm the marine ice sheet instability hypothesis proposed by *Weertman* [1974] and *Thomas and Bentley* [1978]. The hypothesis asserts that physically viable steady profiles for two-dimensional or axisymmetric ice sheets must have their grounding lines located on downward sloping beds.

[107] A caveat to the stability result is that our mathematical model only describes a two-dimensional marine ice sheet, and does not include buttressing through confined three-dimensional ice shelves. Buttressing could serve to stabilize grounding lines on upward sloping beds.

[108] We have also demonstrated that marine ice sheets have discrete steady surface profiles, and neutral equilibrium is not possible. Moreover, marine ice sheets can undergo hysteresis when material parameters (such as ice viscosity, basal slipperiness) or external forcings (accumulation, sea level) are varied. The hysteresis mechanism, which is unique to marine ice sheets, is driven by outflow of ice through the grounding line and requires the presence of an overdeepening. Ice sheet configurations that extend beyond an overdeepening can be forced into irreversible retreat when sea levels rise, accumulation rates drop, or when mean ice temperature rises or bed slipperiness increases. This mode of triggering ice sheet collapse through sea level rise may explain the disappearance of a large ice sheet in the Ross embayment following the Last Glacial Maximum [cf. *Conway et al.*, 1999], and could play a role in causing Heinrich events [*Clarke et al.*, 1999; *Hemming*, 2004; *Flückiger et al.*, 2006]. Conversely, ice sheet profiles with grounding lines at the upstream end of an overdeepening can be forced to advance across the overdeepening if accumulation rates increase, sea levels drop, or when mean ice temperature drops or basal slipperiness decreases.

[109] In arriving at these conclusions, we have also shown that a simplified boundary layer theory for marine ice sheets very closely reproduces results predicted by a more complete marine ice sheet model, and that its predictions can provide a benchmark for numerical marine ice sheet models. In particular, boundary layer theory allows steady ice sheet profiles to be predicted semianalytically, against which numerical results can then be tested. Our results further indicate that significant grid refinement may be necessary to obtain reliable numerical results.

[110] Future research is needed to address three-dimensional effects in marine ice sheet dynamics, such as ice shelf buttressing and ice stream formation. These are probably the most poorly understood components of marine ice sheet dynamics, and are usually modelled using crude parameterizations. Their improved study will require the development of numerical models that are able to track ice stream margins and the grounding line in a three-dimensional marine ice sheet, and this is where research effort should be concentrated.

Appendix A: Numerics

[111] We describe our algorithm in detail in order to facilitate comparison with other numerical methods, and to allow the causes of possible inconsistencies to be traced [see also *Vieli and Payne*, 2005].

[112] In order to deal with the moving boundary $x = x_g$, we use the coordinate stretching

$$\sigma = x/x_g, \qquad \tau = t. \tag{A1}$$

which maps the time-dependent interval $0 < x < x_g(t)$ to the fixed $0 < \sigma < 1$. We introduce τ merely to distinguish between partial derivatives $\partial/\partial t$ and $\partial/\partial \tau$ (taken as x and σ are held constant, respectively). According to the chain rule:

$$\frac{\partial}{\partial x} = \frac{\partial \sigma}{\partial x}\frac{\partial}{\partial \sigma} = \frac{1}{x_g}\frac{\partial}{\partial \sigma} \tag{A2}$$

$$\frac{\partial}{\partial t} = \frac{\partial}{\partial \tau} + \frac{\partial \sigma}{\partial t}\frac{\partial}{\partial \sigma} = \frac{\partial}{\partial \tau} - \frac{\sigma}{x_g}\frac{\mathrm{d}x_g}{\mathrm{d}\tau}\frac{\partial}{\partial \sigma}. \tag{A3}$$

We now deal with the full and simplified models in turn.

A1. Full Model

[113] Under the coordinate stretching, equations (1), (2), (3), (6) and (9) become, respectively,

$$\frac{\partial h}{\partial \tau} - \frac{\sigma}{x_g}\frac{\mathrm{d}x_g}{\mathrm{d}\tau}\frac{\partial h}{\partial \sigma} + \frac{1}{x_g}\frac{\partial (uh)}{\partial \sigma} = a \tag{A4}$$

$$\frac{1}{x_g^{1+1/n}}\frac{\partial}{\partial \sigma}\left[2\bar{A}^{-1/n}h\left|\frac{\partial u}{\partial \sigma}\right|^{1/n-1}\frac{\partial u}{\partial \sigma}\right] - C|u|^{m-1}u - \rho_i g h \frac{1}{x_g}\frac{\partial (h-b)}{\partial \sigma} = 0 \tag{A5}$$

$$\frac{\partial (h-b)}{\partial \sigma} = u = 0 \qquad \text{at} \qquad \sigma = 0 \tag{A6}$$

$$h = (\rho_i/\rho_w)b \qquad \text{at} \qquad \sigma = 1 \tag{A7}$$

$$2\bar{A}^{-1/n}h\frac{1}{x_g^{1/n}}\left|\frac{\partial u}{\partial \sigma}\right|^{1/n-1}\frac{\partial u}{\partial \sigma} = \frac{1}{2}(1-\rho_i/\rho_w)\rho_i g h^2 \qquad \text{at} \quad \sigma = 1. \tag{A8}$$

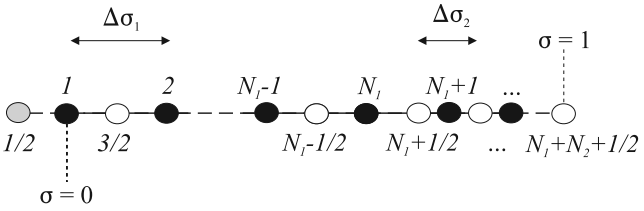

Figure A1. Illustration of the grid used. Solid circles are *h*-grid points, and empty circles are *u*-grid points. The gray circle is the fictitious grid point $\alpha = 1/2$.

[114] We use finite differences with a staggered grid for u and h. (A5) is discretized using centered differences. To stabilize the advection problem (A4) we use an upwind scheme for h as well as a fully implicit time step in u, h and x_g.

[115] Before we discretize, it is important to understand the spatial scales that must be resolved.

[116] Close to the grounding line, the mechanical sheet-shelf transition zone must be resolved. We refine the grid at the grounding line by simply splitting the domain $0 < \sigma < 1$ into two segments, $0 < \sigma < 1 - D$ and $1 - D < \sigma < 1$. D must reflect the transition zone size. Boundary layer theory [*Schoof*, 2007] predicts

$$D \sim \left[8\epsilon/(1-\rho_i/\rho_w)\right]^{n(m+2)/(n+m+3)}, \tag{A9}$$

where

$$\epsilon = \frac{1}{2\bar{A}^{1/n}}\left(\frac{[a]^{2-mn}}{(\rho_i g)^{nm+n-1}C^{n+1}[x]^{(m+1)(n+1)}}\right)^{\frac{1}{n(m+2)}}$$

and $[x]$ and $[a]$ are length and accumulation rate scales for a given ice sheet. ("$\sim$" here means as "a few times this distance.") To give an example of length scales, consider the calculation in Figure 3f: with the parameter values used there and $[a] = a = 0.3$ m a^{-1}, $[x] = 750$ km, we have $D \sim 0.0317$, and the boundary layer physically has a width around $D \times [x] \sim 24$ km. A finer grid can then be chosen in the interval $[1 - D, 1]$ to resolve the boundary layer. (There are more elegant but conceptually more difficult methods of grid refinement, especially ones using a continuous grid refinement with finite elements.)

[117] Equations (A4) and (A5) hold in $(0, 1 - D)$ and $(1 - D, 1)$. At $\sigma = 1 - D$, h, u and $\partial u/\partial\sigma$ (i.e., ice thickness, velocity and stress) must be continuous.

[118] We define a uniformly spaced staggered grid for h and u in each subdomain, with N_1 grid points for h and u in $[0, 1 - D]$, and N_2 grid points in $(1 - D, 1]$. The junction $\sigma = 1 - D$ is taken as a *u*-grid point, as is the grounding line at $\sigma = 1$. The ice divide $\sigma = 0$ is an *h*-grid point (Figure A1). We label *h*-grid points by indices $\alpha = 1,2,\ldots, N_1 + N_2$, and *u*-grid points by indices $\alpha = 3/2, 5/2,\ldots, N_1 + N_2 + 1/2$. $\alpha = N + 1/2$ is the junction at $\sigma = 1 - D$. The spacing between *h*-grid points (or *u*-grid points) with $1 \le \alpha \le N_1 + 1/2$ is then

$$\Delta\sigma_1 = \frac{1-D}{N_1 - 1/2}, \tag{A10}$$

and

$$\Delta\sigma_2 = \frac{D}{N_2} \tag{A11}$$

for $N_1 + 1/2 \le \alpha \le N_1 + N_2 + 1/2$. The positions of grid points are

$$\sigma_\alpha = (\alpha - 1)\Delta\sigma_1$$

if $1 \le \alpha \le N_1 + 1/2$, and

$$\sigma_\alpha = \left(N_1 - \frac{1}{2}\right)\Delta\sigma_1 + \left(\alpha - N_1 - \frac{1}{2}\right)\Delta\sigma_2$$

if $N_1 + 1/2 < \alpha < N_1 + N_2 + 1/2$.

[119] Indices i and j will be restricted to integer values. A constant time step $\Delta\tau$ is used, and $h_i^j = h(\sigma_i, j\Delta t)$. Similarly, $u_{i+1/2}^j = u(\sigma_{i+1/2}, j\Delta\ t)$, $x_g^j = x_g(j\Delta t)$ denotes the value of x_g at $\tau = j\Delta\tau$. Moreover, we define ice sheet bed depth b as $b_i^j = b(x_g^j\sigma_i)$ for $i = 1,\ldots N_1 + N_2$, and $b_g^j = b(x_g^j)$ (the bed does not change under the coordinate stretching, so argument of b here is x, not σ!). Similarly, $a_i^j = a(x_g^j\sigma_i, h_i^j - b_i^j)$, assuming a to be a function of unstretched position x and ice surface elevation $h - b$.

[120] For $1 \le i \le N_1 - 1$, equation (A5) is discretized as

$$\begin{aligned}\frac{2\bar{A}^{-1/n}}{\left(x_g^j\Delta\sigma_1\right)^{1+1/n}}\cdot\Big[&h_{i+1}^j|u_{i+3/2}^j - u_{i+1/2}^j|^{1/n-1}\left(u_{i+3/2}^j - u_{i+1/2}^j\right)\\ &- h_i^j|u_{i+1/2}^j - u_{i-1/2}^j|^{1/n-1}\left(u_{i+1/2}^j - u_{i-1/2}^j\right)\Big]\\ &- C|u_{i+1/2}^j|^{m-1}u_{i+1/2}^j\\ &- \frac{1}{2}\rho_i g\left(h_i^j + h_{i+1}^j\right)\frac{h_{i+1}^j - b_{i+1}^j - h_i^j + b_i^j}{x_g^j\Delta\sigma_1} = 0.\end{aligned} \tag{A12}$$

For $i = 1$, this involves the fictitious grid point $\alpha = i - 1/2 = 1/2$, located at $\sigma = -\Delta\sigma_1/2$. By symmetry, the velocity at this grid point must be equal in magnitude and opposite in direction to velocity at $\sigma_{3/2} = \Delta\sigma_1/2$. In other words, we assign $u_{1/2} = -u_{3/2}$. This also takes care of the boundary condition (A6). For $N_1 + 1 \le i \le N_1 + N_2 - 1/2$, (A5) is discretized analogously to (A11): we simply replace $\Delta\sigma_1$ by $\Delta\sigma_2$ in (A11).

[121] For the junction between the two subdomains, continuity in u is automatically assured because a *u*-grid point is located there. Continuity in $\partial u/\partial\sigma$ (and hence stress) requires

$$\frac{u_{N_1+3/2}^j - u_{N_1+1/2}^j}{\Delta\sigma_2} - \frac{u_{N_1+1/2}^j - u_{N_1-1/2}^j}{\Delta\sigma_1} = 0. \tag{A13}$$

Equation (A8), substituting for ice thickness with the help of (A7), can be cast as

$$\begin{aligned}2\bar{A}^{-1/n}&\frac{|u_{N_1+N_2+1/2}^j - u_{N_1+N_2-1/2}^j|^{1/n-1}}{\left(x_g^j\Delta\sigma_2\right)^{1/n}}\\ &\cdot\left(u_{N_1+N_2+1/2}^j - u_{N_1+N_2-1/2}^j\right) - \frac{1}{2}(1-\rho_i/\rho_w)\rho_w g b_g^j = 0.\end{aligned} \tag{A14}$$

[122] Equation (A4) is discretized using an upwind scheme with a backward Euler step, with a centered

difference for the "advection term" that arises because of coordinate stretching (as the relevant upwind direction would depend on the sign of $\mathrm{d}x_g/\mathrm{d}\tau$). For $1 < i < N_1$,

$$\frac{h_i^j - h_i^{j-1}}{\Delta\tau} - \frac{\sigma_i\left(x_g^j - x_g^{j-1}\right)\left(h_{i+1}^j - h_{i-1}^j\right)}{2\Delta\tau\Delta\sigma_1 x_g^j} + \frac{h_i^j\left(u_{i+1/2}^j - u_{i-1/2}^j\right) - h_{i-1}^j\left(u_{i-1/2}^j + u_{i-3/2}^j\right)}{2x_g^j\Delta\sigma_1} - a_i^j = 0. \quad \text{(A15)}$$

Again, the expression on the left-hand side involves $u_{1/2}$ for $i = 1$, and we identify $u_{1/2} = -u_{3/2}$. For $i = 1$, symmetry at the ice divide demands

$$\frac{h_1^j - h_1^{j-1}}{\Delta\tau} + \frac{2h_1^j u_{3/2}^j}{\Delta\sigma_1 x_g^j} + a_1^j = 0. \quad \text{(A16)}$$

For $i = N_1$, we replace the centered difference in the coordinate stretching term by a one-sided difference:

$$\frac{h_{N_1}^j - h_{N_1}^{j-1}}{\Delta\tau} - a_{N_1}^j - \frac{\sigma_i\left(x_g^j - x_g^{j-1}\right)\left(h_{N_1}^j - h_{N_1-1}^j\right)}{\Delta\tau\Delta\sigma_2 x_g^j} + \frac{h_{N_1}^j\left(u_{N_1+1/2}^j + u_{N_1-1/2}^j\right) - h_{N_1-1}^j\left(u_{N_1-1/2}^j + u_{N_1-3/2}^j\right)}{2x_g^j\Delta\sigma_1} = 0. \quad \text{(A17)}$$

This is done consistently with (A18) below, which extrapolates the slope between $i = N_1-1$ and $i = N_1$ onto the junction between the two domains.

[123] For $N_1 + 1 < i < N_1 + N_2$, (A4) is discretized the same as (A15): again, we simply replace $\Delta\sigma_1$ by $\Delta\sigma_2$ in (A4). For $i = N_1 + N_2$, the centered difference used in the second term in (A4) is again replaced by a one-sided difference at $i = N_1 + N_2$ as in (A17): we simply replace $\Delta\sigma_1$ by $\Delta\ \sigma_2$ in (A17), and we replace N_1 in the indices by $N_1 + N_2$.

[124] To ensure continuity of thickness at the junction between the domains at $\sigma = 1 - D$, we require that the linear extrapolation of h from the grid points $\alpha = N_1 - 1$ and $\alpha = N_1$ to the grid point $\alpha = N_1 + 1$ match $h_{N_1+1}^j$ (Figure A1). In other words,

$$(3 + \Delta\sigma_2/\Delta\sigma)h_{N_1}^j - (1 + \Delta\sigma_2/\Delta\sigma)h_{N_1-1}^j - h_{N_1+1}^j = 0. \quad \text{(A18)}$$

[125] It remains to impose the flotation condition (A7). Again, we require that the linear extrapolation from $\alpha = N_1 + N_2 - 1$ and $\alpha = N_1 + N_2$ onto $\alpha = N_1 + N_2 + 1/2$ should match the flotation thickness $\rho_w b_g^j/\rho_i$:

$$3h_{N_1+N_2}^j - h_{N_1+N_2-1}^j - (\rho_w/\rho_i)b_g^j = 0. \quad \text{(A19)}$$

[126] By contrast with the numerical algorithms discussed by *Vieli and Payne* [2005], we do not differentiate the flotation condition in (A7) with respect to τ to obtain an explicit evolution equation for x_g, but retain it in its initial form. This is simple to do because of the coordinate stretching employed here, and because of the implicit time step. The main advantage of using (A19) compared with its differentiated form is that there is no drift in computed ice thickness at the grounding line from the flotation condition.

[127] (A19) also completes the discretized set of equations to be solved at every time step. Equations (A11)–(A14) constitute $N_1 + N_2$ nonlinear equations, while (A15)–(A18) constitute another $N_1 + N_2$ equations, so that together with (A19) we have a total of $2(N_1 + N_2) + 1$ equations. This matches the number of unknowns: we solve for $N_1 + N_2$ variables $u_{i+1/2}^j$ and $N_1 + N_2$ variables h_i^j, where j is fixed and i ranges from 1 to $N_1 + N_2$, as well as for x_g^j. The other variables appearing in (A11)–(A19) are themselves functions of these dependent variables, for instance the a_i^j's and b_i^js.

[128] (A11)–(A19) equations can then be solved using a variety of nonlinear solvers. In this paper, we use a standard Newton iteration. Computing the relevant (sparse) Jacobian is a straightforward if tedious task. The time step Δt is generally limited by the higher resolution and higher ice velocity in the transition zone.

A2. Simplified Models

[129] We deal only with model B; model A can be discretized analogously. Again, we apply the coordinate stretching given by equation (A1), and transform equation (13) accordingly. Again we split the domain into $[0, 1 - D]$ and $[1 - D, 1]$, this time to resolve the steep ice surface slope near the grounding line. On each subdomain we define a regular grid with N_1 and N_2 grid points, with spacing $\Delta\sigma_1 = (1 - D)/(N_1-1)$ and $\Delta\sigma_2 = D/N_2$. The transformed version of (13) is discretized using centered differences and an implicit time step. The spatial discretization can be recognized as a type-I scheme in the terminology of *Huybrechts et al.* [1996]. For $1 < i < N_1$,

$$\frac{h_i^j - h_i^{j-1}}{\Delta\tau} - \frac{\sigma_i\left(x_g^j - x_g^{j-1}\right)\left(h_{i+1}^j - h_{i-1}^j\right)}{2\Delta\tau\Delta\sigma_1 x_g^j} - \left(\frac{\rho_i g}{C}\right)^{\frac{1}{m}} \frac{1}{\left(x_g^j\Delta\sigma_1\right)^{\frac{1}{m}+1}} \cdot \left\{\left[\frac{h_i^j + h_{i+1}^j}{2}\right]^{\frac{1}{m}+1} \times |h_{i+1}^j - b_{i+1}^j - h_i^j + b_i^j|^{\frac{1}{m}-1} \cdot \left(h_{i+1}^j - b_{i+1}^j - h_i^j + b_i^j\right) - \left[\frac{h_i^j + h_{i-1}^j}{2}\right]^{\frac{1}{m}+1} \cdot |h_i^j - b_i^j - h_{i-1}^j + b_{i-1}^j|^{\frac{1}{m}-1} \cdot \left(h_i^j - b_i^j - h_{i-1}^j + b_{i-1}^j\right)\right\} = a_i^j, \quad \text{(A20)}$$

and similarly for $N_1 < i < N1 + N_2$, but with $\Delta\sigma_1$ replaced by $\Delta\sigma_2$. The notation for h_i^j, b_i^j and x_g^j is the same as for the full model. Equation (A20) holds for $1 < i < N$. At the ice divide, vanishing surface slope gives

$$\frac{h_2^j - b_2^j - h_1^j + b_1^j}{\Delta\sigma_1} = 0. \quad \text{(A21)}$$

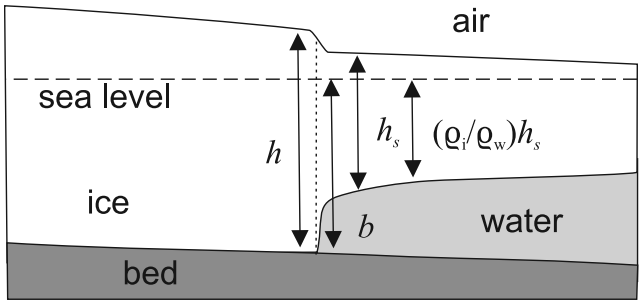

Figure B1. Geometry for calculating stresses at the grounding line. If the shelf is perfectly afloat, then the base of the shelf is at $(\rho_i/\rho_w)h_s$ below sea level.

At the junction between the domains, we require flux continuity:

$$\left[\frac{h^j_{N_1-1}+h^j_{N_1}}{2}\right]^{\frac{1}{m}+1}|h^j_{N_1}-b^j_{N_1}-h^j_{N_1-1}+b^j_{N_1-1}|^{\frac{1}{m}-1}\cdot\left(h^j_{N_1}-b^j_{N_1}-h^j_{N_1-1}+b^j_{N_1-1}\right)-\left[\frac{h^j_{N_1}+h^j_{N_1+1}}{2}\right]^{\frac{1}{m}+1}|h^j_{N_1+1}-b^j_{N_1+1}-h^j_{N_1}+b^j_{N_1}|^{\frac{1}{m}-1}\cdot\left(h^j_{N_1+1}-b^j_{N_1+1}-h^j_{N_1}+b^j_{N_1}\right)=0. \tag{A22}$$

At the grounding line, we have a flotation and a flux condition:

$$h^j_{N_1+N_2}-\frac{\rho_w}{\rho_i}b^j_{N_1+N_2}=0, \tag{A23}$$

$$\frac{1}{\left(x^j_g\Delta\sigma\right)^{\frac{1}{m}}}\left[\frac{h^j_{N_1+N_2}+h^j_{N_1+N_2-1}}{2}\right]^{\frac{1}{m}+1}\cdot|h^j_{N_1+N_2}-b^j_{N_1+N_2}-h^j_{N_1+N_2-1}+b^j_{N_1+N_2-1}|^{\frac{1}{m}-1}\cdot\left(h^j_{N_1+N_2}-b^j_{N_1+N_2}-h^j_{N_1+N_2-1}+b^j_{N_1+N_2-1}\right)-\left(\frac{\bar{A}(\rho_i g)^{n+1}(1-\rho_i/\rho_w)^n}{4^nC}\right)^{\frac{1}{m+1}}\left(h^j_{N_1+N_2}\right)^{\frac{m+n+3}{m+1}}=0. \tag{A24}$$

We have $N_1 + N_2 + 1$ nonlinear equations for the $N_1 + N_2$ h^j_is and x^j_g, and once again we use a Newton iteration scheme to solve them.

Appendix B: Grounding Line Stresses for Discontinuous Ice Thickness

[130] Consider the balance of horizontal forces at the grounding line when the ice thickness on the grounded side is greater than flotation thickness, and less on the shelf side (as discussed in section 4.3). Let shelf thickness at the grounding line be h_s and grounded ice thickness h. Depth-integrated longitudinal stress F_d in the shelf is then (cf. the derivation of equation (9))

$$F_d=\frac{1}{2}\rho_i\left(1-\frac{\rho_i}{\rho_w}\right)gh_s^2,$$

defining forces oriented in the x direction to be positive. Cryostatic pressure in the shelf also contributes a term

$$F_s=-\int_0^{h_s}\rho g z'\,\mathrm{d}z'=\frac{1}{2}\rho_i g h_s^2,$$

negative because it acts in the negative x direction. In addition, the hydrostatic pressure in the ocean exerts a force on the vertical part of the shelf bottom at the grounding line. This submarine cliff extends from a depth $\rho_i h_s/\rho_w$ to a depth b below sea level (see Figure B1). The contribution of hydrostatic water pressure to force balance is therefore

$$F_o=-\int_{(\rho_i/\rho_w)h_s}^{b}\rho w g z'\,\mathrm{d}z'=-\frac{1}{2}\rho_w g b^2+\frac{1}{2}\rho_i g h_s^2.$$

On the grounded side, cryostatic pressure contributes

$$F_g=\frac{1}{2}\rho_i g h^2,$$

while depth-integrated longitudinal stress on the grounded side of the grounding line contributes a term

$$F_l=-2\bar{A}^{-1/n}h\left|\frac{\partial u}{\partial x}\right|^{1/n-1}\frac{\partial u}{\partial x}.$$

Force balance at the grounding line requires that these contributions sum to zero:

$$0=F_d+F_s+F_o+F_g+F_l=-\frac{1}{2}\rho_w g b^2+\frac{1}{2}\rho_i g h^2-2\bar{A}^{-1/n}h\left|\frac{\partial u}{\partial x}\right|^{1/n-1}\frac{\partial u}{\partial x}. \tag{B1}$$

Hence

$$2\bar{A}^{-1/n}h\left|\frac{\partial u}{\partial x}\right|^{1/n-1}\frac{\partial u}{\partial x}=\frac{1}{2}\rho_i g h^2-\frac{1}{2}\rho_w g b^2. \tag{B2}$$

[131] **Acknowledgments.** This work was supported by the U.S. National Science Foundation through grant DMS-03227943. Additional resources were provided by the Canadian Foundation for Climate and Atmospheric Science through the Polar Climate Stability Network. Discussions with Garry Clarke, Tim Creyts, Andrew Fowler, Dan Goldberg, David Holland, Sophie Nowicki, Dave Pollard, Maureen Raymo, Alan Rempel, Alex Wilchinsky, Duncan Wingham, and Grae Worster and the constructive comments of Frank Pattyn, Richard Hindmarsh, and Tavi Murray are gratefully acknowledged.

References

Bindschadler, R. A. (2006), Hitting the ice sheets where it hurts, *Science*, *311*, 1720–1721.

Chugunov, V. A., and A. V. Wilchinsky (1996), Modelling of marine glacier and ice-sheet-ice-shelf transition zone based on asymptotic analysis, *Ann. Glaciol.*, *23*, 59–67.

Clarke, G. K. C., S. J. Marshall, C. Hillaire-Marcel, G. Bilodeau, and C. Veiga-Pires (1999), A glaciological perspective on Heinrich events, in *Mechanisms of Global Climate Change at Millennial Time Scales*, *Geophys. Monogr. Ser.*, vol. 112, edited by L. D. Keigwin, C. U. Clark, and R. S. Webb, pp. 143–262, AGU, Washington, D. C.

Conway, H., B. L. Ball, G. H. Denton, A. M. Gades, and E. D. Waddington (1999), Past and future grounding-line retreat of the west Antarctic ice sheet, *Science*, *286*, 280–283.

Dupont, T. K., and R. B. Alley (2005), Assessment of the importance of ice-shelf buttressing to ice-sheet flows, *Geophys. Res. Lett.*, *32*, L04503, doi:10.1029/2004GL022024.

Flückiger, J. R., R. Knutti, and J. W. C. White (2006), Oceanic processes as potential trigger and amplifying mechanisms for Heinrich events, *Paleoceanography*, *21*, PA2014, doi:10.1029/2005PA001204.

Fowler, A. C. (1981), A theoretical treatment of the sliding of glaciers in the absence of cavitation, *Philos. Trans. R. Soc. London, Ser. A*, *298*, 637–685.

Hemming, S. R. (2004), Heinrich events: Massive late Pleistocene detritus layers of the North Atlantic and their global imprint, *Rev. Geophys.*, *42*, RG1005, doi:10.1029/2003RG000128.

Herterich, K. (1987), On the flow within the transition zone between ice sheet and ice shelf, in *Dynamics of the West Antarctic Ice Sheet: Proceedings of a Workshop Held in Utrecht, May 6–8, 1985*, edited by C. J. van der Veen and J. Oerlemans, pp. 185–202, Springer, New York.

Hindmarsh, R. C. A. (1993), *Qualitative dynamics of marine ice sheets, in Ice in the Climate System*, edited by W. R. Peltier, pp. 67–99, Springer, New York.

Hindmarsh, R. C. A. (1996), Stability of ice rises and uncoupled marine ice sheets, *Ann. Glaciol.*, *23*, 94–104.

Hindmarsh, R. C. A. (2006), The role of membrane-like stresses in determining the stability and sensitivity of the Antarctic ice-sheets: Back-pressure and grounding-line motion, *Philos. Trans. R. Soc. London, Ser. A*, *364*, 1733–1767, doi:10.1098/rsta.2006.1797.

Hindmarsh, R. C. A., and E. LeMeur (2001), Dynamical processes involved in the retreat of marine ice sheets, *J. Glaciol.*, *47*, 271–282.

Holland, D. M. (2002), Computing marine-ice thickness at an ice-shelf base, *J. Glaciol.*, *48*, 9–19.

Holland, D. M., and A. Jenkins (2001), Adaptation of an isopycnic coordinate ocean model for the study of circulation beneath ice shelves, *Mon. Weather Rev.*, *129*, 1905–1927.

Howat, I. M., I. Joughin, S. Tulaczyk, and S. Gogineni (2005), Rapid retreat and acceleration of Helheim Glacier, east Greenland, *Geophys. Res. Lett.*, *32*, L22502, doi:10.1029/2005GL024737.

Hulbe, C. L., D. R. MacAyeal, G. H. Denton, J. Kleman, and T. V. Lowell (2004), Catastrophic ice shelf breakup as the source of Heinrich event icebergs, *Paleoceanography*, *19*, PA1004, doi:10.1029/2003PA000890.

Huybrechts, P., T. Payne, and EISMINT Intercomparison Group (1996), EISMINT benchmarks for testing ice-sheet models, *Ann. Glaciol.*, *23*, 1–12.

Luckman, A., T. Murray, R. de Lange, and E. Hanna (2006), Rapid and synchronous ice-dynamic changes in East Greenland, *Geophys. Res. Lett.*, *33*, L03503, doi:10.1029/2005GL025428.

MacAyeal, D. R. (1987), Ice-shelf backpressure: Form drag versus dynamics drag, in *Dynamics of the West Antarctic Ice Sheet: Proceedings of a Workshop Held in Utrecht, May 6–8, 1985*, edited by C. J. van der Veen and J. Oerlemans, pp. 141–160, Springer, New York.

MacAyeal, D. R. (1989), Large-scale flow over a viscous basal sediment: Theory and application to Ice Stream E, Antarctica, *J. Geophys. Res.*, *94*, 4017–4087.

MacAyeal, D. R. (1993), Binge/purge oscillations of the Laurentide Ice Sheet as a cause of North Atlantic Heinrich events, *Paleoceanography*, *8*, 775–784.

MacAyeal, D. R., and V. Barcilon (1988), Ice-shelf response to ice-stream discharge fluctuations: I. Unconfined ice tongues, *J. Glaciol.*, *34*, 121–127.

Meier, M. F., and A. Post (1987), Fast tidewater glaciers, *J. Geophys. Res.*, *92*, 9051–9058.

Muszynski, I., and G. E. Birchfield (1987), A coupled marine ice-stream-ice-shelf model, *J. Glaciol.*, *33*, 3–15.

Oerlemans, J. (2002), Global dynamics of the Antarctic ice sheet, *Clim. Dyn.*, *19*, 85–93.

Oerlemans, J., and F. M. Nick (2005), A minimal model of a calving glacier, *Ann. Glaciol.*, *42*, 1–6.

Oerlemans, J., and F. M. Nick (2006), Modelling the advance-retreat cycle of a tidewater glacier using simple sediment dynamics, *Global Planet. Change*, *50*, 148–160, doi:10.1016/j.gloplacha.2005.12.002.

Paterson, W. S. B. (1994), *The Physics of Glaciers*, 3rd ed., Elsevier, New York.

Pattyn, F., A. Huyghe, S. De Brabander, and B. De Smedt (2006), Role of transition zones in marine ice sheet dynamics, *J. Geophys. Res.*, *111*, F02004, doi:10.1029/2005JF000394.

Payne, A. J., A. Vieli, A. P. Shepherd, D. J. Wingham, and E. Rignot (2004), Recent dramatic thinning of the largest West Antarctic ice stream triggered by oceans, *Geophys. Res. Lett.*, *31*, L23401, doi:10.1029/2004GL021284.

Rignot, E., D. G. Vaughan, M. Schmeltz, T. Dupont, and D. MacAyeal (2002), Acceleration of Pine Island and Thwaites glaciers, West Antarctica, *Ann. Glaciol.*, *34*, 189–194.

Rignot, E., G. Casassa, S. Gogineni, W. Krabill, A. Rivera, and R. Thomas (2004), Accelerated ice discharge from the Antarctic Peninsula following the collapse of Larsen B ice shelf, *Geophys. Res. Lett.*, *31*, L18401, doi:10.1029/2004GL020697.

Schmeltz, M., E. Rignot, T. K. Dupont, and D. R. MacAyeal (2002), Sensitivity of Pine Island Glacier, West Antarctica, to changes in ice-shelf and basal conditions: A model study, *J. Glaciol.*, *48*, 552–558.

Schoof, C. (2006), A variational approach to ice-stream flow, *J. Fluid Mech.*, *556*, 227–251.

Schoof, C. (2007), Marine ice sheet dynamics. part I. The case of rapid sliding, *J. Fluid Mech.*, *573*, 27–55.

Shumskiy, P. A., and M. S. Krass (1976), Mathematical models of ice shelves, *J. Glaciol.*, *17*, 419–432.

Stone, J. O., G. A. Balco, D. E. Sugden, M. W. Caffee, L. C. Sass III, S. G. Cowdery, and C. Siddoway (2003), Holocene deglaciation of Marie Byrd Land, West Antarctica, *Science*, *299*, 99–102.

Thomas, R. H., and C. R. Bentley (1978), A model for Holocene retreat of the West Antarctic ice sheet, *Quat. Res.*, *10*, 150–170.

van der Veen, C. J. (1985), Response of a marine ice sheet to changes at the grounding line, *Quat. Res.*, *24*, 257–267.

van der Veen, C. J. (1996), Tidewater calving, *J. Glaciol*, *42*, 375–385.

Vaughan, D. G., H. F. J. Corr, F. Ferraccioli, N. Frearson, A. O'Hare, D. Mach, J. W. Holt, D. D. Blankenship, D. L. Morse, and D. A. Young (2006), New boundary conditions for the West Antarctic ice sheet: Subglacial topography beneath Pine Island Glacier, *Geophys. Res. Lett.*, *33*, L09501, doi:10.1029/2005GL025588.

Vieli, A., and A. J. Payne (2005), Assessing the ability of numerical ice sheet models to simulate grounding line migration, *J. Geophys. Res.*, *110*, F01003, doi:10.1029/2004JF000202.

Vieli, A., M. Funk, and H. Blatter (2001), Flow dynamics of tidewater glaciers: Numerical modelling approach, *J. Glaciol.*, *47*, 595–606.

Weertman, J. (1957), On the sliding of glaciers, *J. Glaciol.*, *3*, 33–38.

Weertman, J. (1974), Stability of the junction of an ice sheet and an ice shelf, *J. Glaciol.*, *13*, 3–13.

Wellner, J. S., A. L. Lowe, S. S. Ship, and J. B. Anderson (2001), The distribution of glacial geomorphic features on the Antarctic continental shelf and correlation with substrate, implications for ice behaviour, *J. Glaciol.*, *47*, 397–411.

C. Schoof, Department of Earth and Ocean Sciences, University of British Columbia, 6339 Stores Road, Vancouver, BC, Canada V6T 1Z4. (cschoof@eos.ubc.ca)